Resource

Cell Chemical Biology

# Humanized zebrafish as a tractable tool for *in vivo* evaluation of pro-myelinating drugs

## Graphical abstract

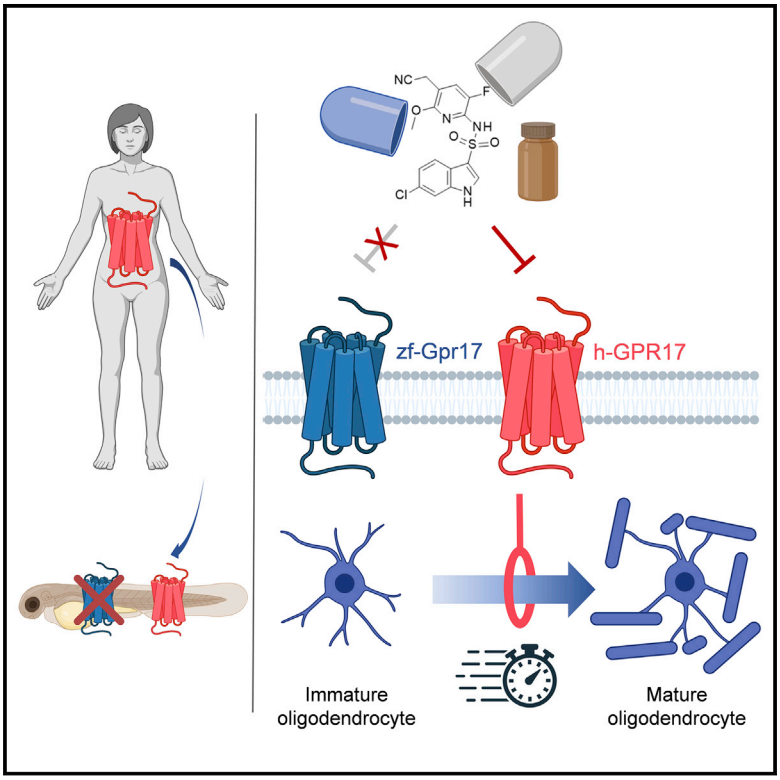


## Highlights

- Gpr17 expression and function in oligodendrocytes are conserved from zebrafish to mammals
- Human (h)-GPR17 efficiently replaces the zebrafish ortholog in the *in vivo* context
- An h-GPR17 antagonist mimics the *gpr17*-null fish phenotype in GPR17-humanized zebrafish
- Proof of principle of GPR17-humanized zebrafish for pro-remyelination drug discovery

## Authors

Felix Häberlein, Enrico Mingardo, Nicole Merten, ..., Benjamin Odermatt, Evi Kostenis, Jesus Gomeza

## Correspondence

b.odermatt@uni-bonn.de (B.O.), kostenis@uni-bonn.de (E.K.), jgomeza@uni-bonn.de (J.G.)

## In brief

The identification of drugs that promote remyelination in patients with demyelinating diseases, such as multiple sclerosis, is in high demand. Häberlein et al. introduce a GPR17-humanized zebrafish as proof of principle that fosters *in vivo* identification of novel pro-remyelination compounds acting via targeted inhibition of human GPR17.

Häberlein et al., 2022, Cell Chemical Biology *29*, 1541–1555
October 20, 2022 
https://doi.org/10.1016/j.chembiol.2022.08.007

CellPress

Cell Chemical Biology

CellPress

Resource

# Humanized zebrafish as a tractable tool for *in vivo* evaluation of pro-myelinating drugs

Felix Häberlein,[1,2,7] Enrico Mingardo,[2,7] Nicole Merten,[1] Nina-Katharina Schulze Köhling,[1,2] Philip Reinoß,[2] Katharina Simon,[1] Anna Japp,[3] Bhuvaneswari Nagarajan,[2] Ramona Schrage,[4] Cecile Pegurier,[4] Michel Gillard,[4] Kelly R. Monk,[5] Benjamin Odermatt,[2,6,*] Evi Kostenis,[1,8,*] and Jesus Gomeza[1,*]

[1]Molecular, Cellular, and Pharmacobiology Section, Institute of Pharmaceutical Biology, University of Bonn, 53115 Bonn, Germany
[2]Institute of Anatomy, Division of Anatomy and Cell Biology, University Clinics, University of Bonn, 53115 Bonn, Germany
[3]Institute of Neuropathology, University Clinics, University of Bonn, 53127 Bonn, Germany
[4]UCB Biopharma, CNS Research, 1420 Braine-l'Alleud, Belgium
[5]Vollum Institute, Oregon Health & Science University, Portland, OR 97239, USA
[6]Institute of Anatomy, Division of Neuroanatomy, University Clinics, University of Bonn, 53115 Bonn, Germany
[7]These authors contributed equally
[8]Lead contact
*Correspondence: b.odermatt@uni-bonn.de (B.O.), kostenis@uni-bonn.de (E.K.), jgomeza@uni-bonn.de (J.G.)
https://doi.org/10.1016/j.chembiol.2022.08.007

## SUMMARY

Therapies that promote neuroprotection and axonal survival by enhancing myelin regeneration are an unmet need to prevent disability progression in multiple sclerosis. Numerous potentially beneficial compounds have originated from phenotypic screenings but failed in clinical trials. It is apparent that current cell- and animal-based disease models are poor predictors of positive treatment options, arguing for novel experimental approaches. Here we explore the experimental power of humanized zebrafish to foster the identification of pro-remyelination compounds via specific inhibition of GPR17. Using biochemical and imaging techniques, we visualize the expression of zebrafish (*zf*)-*gpr17* during the distinct stages of oligodendrocyte development, thereby demonstrating species-conserved expression between zebrafish and mammals. We also demonstrate species-conserved function of zf-Gpr17 using genetic loss-of-function and rescue techniques. Finally, using *GPR17*-humanized zebrafish, we provide proof of principle for *in vivo* analysis of compounds acting via targeted inhibition of human GPR17. We anticipate that *GPR17*-humanized zebrafish will markedly improve the search for effective pro-myelinating pharmacotherapies.

## INTRODUCTION

Myelin is a protective lipid sheath made by matured oligodendrocytes that encompasses and insulates neuronal axons, thus ensuring rapid propagation of action potentials (Marinelli et al., 2016). Damage to myelin causes severe neurological deficits (Fields, 2008; Shukla et al., 2021) and is a hallmark feature of demyelinating diseases such as multiple sclerosis (MS) (Filippi et al., 2018), in which myelin sheaths are damaged by autoreactive B and T cells. This disruptive process is followed by the endogenous attempt of the central nervous system (CNS) to repair the defective myelin sheath, a process referred to as remyelination (Fancy et al., 2011; Dendrou et al., 2015). Current treatments for MS typically target immune functions to reduce CNS inflammation and thereby lessen disease severity, slow down disease progression, and decrease relapse rates, which are characteristic clinical features of MS (Lubetzki et al., 2020). A second avenue in MS treatment is to facilitate myelin regeneration and thereby enhance axonal survival and neuroprotection (Franklin and Ffrench-Constant, 2017; Bebo et al., 2022). Consequently, the development of novel therapeutic agents that promote remyelination has become an active area of research. Phenotypic screenings have discovered a large number of potential pro-remyelination compounds, both repurposed and new, that enhance oligodendrocyte differentiation and maturation (Lubetzki et al., 2020; Balestri et al., 2021). However, only a few of them have finally reached phase 2 clinical trials, and only one, clemastine, a histamine H1 receptor antagonist, has shown some promising results in patients with optic neuritis, a common symptom of MS (Green et al., 2017). Consequently, none of the currently approved disease-modifying treatments for MS is designed to promote remyelination (Balashov, 2020) and, therefore, therapeutic development for MS that aims to halt disability progression continues to be the key unmet need (Lubetzki et al., 2020).

Phenotypic drug discovery comes with inherent challenges often related to the identification of compounds for unknown protein targets and/or with unknown mechanism of action, or related to the use of cell-based assays, which are unable to capture the effects of small molecules on oligodendrocyte biology

and myelination (Moffat et al., 2017). As a solution, whole-organism assays can be employed, but typical rodent models that offer deeper insights into activity and toxicity cannot be screened at scale. For all the above reasons, a successful drug discovery program to foster myelin regeneration should ideally merge (1) knowledge of specific protein targets that are disease modifying with (2) whole-organism screening to address the complexity of *in vivo* physiology and the dynamic interactions that cause a demyelinating disease. Furthermore, an essential point to consider is that experimental drugs are required to function across animal species, since they are ultimately expected to enhance the human oligodendrocyte maturation process. Unfortunately, potential drugs emerging from rodent MS studies have had a poor record of success in clinical trials, indicating the limitations of this approach (Baker and Amor, 2015). Therefore, new and more "humanized" animal models, in which human genes previously identified as targets for therapeutic intervention in MS are introduced and expressed, are being embraced for the identification of novel compounds with pro-myelination effects (Friese et al., 2006; Ben-Nun et al., 2014; Lassmann and Bradl, 2017).

Zebrafish (*Danio rerio*) has evolved into a popular model vertebrate for the study of developmental processes and drug testing (Taylor et al., 2010; Chen et al., 2020; Patton et al., 2021). In particular, zebrafish larvae have been established for the *in vivo* study of oligodendrocyte biology and myelination (Preston and Macklin, 2015; Ackerman and Monk, 2016; Czopka, 2016), but also for phenotypic screens of pro-myelination compounds (Buckley et al., 2010; Early et al., 2018). Here, we took advantage of the experimental and genetic power of the zebrafish and introduce a humanized zebrafish as a proof of principle that fosters the identification of pro-remyelination compounds. As the protein target we selected GPR17, an orphan G-protein-coupled receptor (GPCR) and integral component of the signaling program that modulates the timing of oligodendrocyte differentiation. GPR17 acts as an inhibitor of oligodendrocyte maturation, orchestrating the transition between immature pre-myelinating and mature myelinating oligodendrocytes (Chen et al., 2009; Simon et al., 2016; Merten et al., 2018). GPR17 is highly abundant within active white matter plaques of MS patients as well as in mouse models of drug- and injury-induced demyelination (Chen et al., 2009; Ou et al., 2016; Wang et al., 2020). Genetic deletion of *Gpr17* in mice not only protects from lysolecithin-induced demyelination but also accelerates remyelination after lysolecithin injury (Ou et al., 2016). Consequently, there is a general consensus that GPR17 plays a crucial role in MS, acting as an oligodendroglial differentiation inhibitor that impairs the remyelination process, and that its pharmacological inhibition would promote remyelination on demyelinated axons (Mogha et al., 2016; Merten et al., 2018; Dziedzic et al., 2020).

In this study, we examined in zebrafish whether *gpr17* is expressed in oligodendrocyte-lineage cells and conserves its functional role as an inhibitor of oligodendrocyte maturation using different zebrafish reporter lines combined with imaging and genetic loss-of-function and rescue techniques. Subsequently, we expressed human *GPR17* in zebrafish and evaluated the extrapolative capabilities of the *GPR17*-humanized zebrafish as an *in vivo* system for the analysis of compounds acting via targeted inhibition of human GPR17.

## RESULTS

### *gpr17* is expressed during oligodendrocyte development in zebrafish

We identified in the Ensembl genome browser (www.ensembl.org) the predicted *gpr17* gene, which maps on zebrafish chromosome 6 and was originally named si:ch73-194h10.4 (ZDB-GENE-100922-133; ZFIN.org). The predicted gene consists of one exon containing a 1,020-bp open reading frame that is translated into a Gpr17 protein of 339 amino acids. Simple Modular Architecture Research Tool (SMART) analysis predicted that zf-Gpr17 would share the common structural signature of GPCRs, with seven hydrophobic transmembrane segments, an extracellular amino terminus, and an intracellular carboxyl terminus. Comparison between zf-Gpr17 and its orthologs showed a 56% amino acid similarity with human and 54% with mouse and rat GPR17 (Figure S1). We analyzed the *gpr17* sequence upon PCR amplification from genomic DNA, confirming that the gene is intronless in its coding region. Furthermore, the transcriptional start site on *gpr17* mRNA was analyzed by rapid amplification of cDNA 5′ ends (RACE), which identified a 5′ flanking region of 104 bp located 6,282 nucleotides upstream of the receptor start codon (Figure S2). Therefore, the *zf-gpr17* gene consists of two exons separated by a 6,273-bp intron, with the open reading frame being located on the second exon (Figure 1A).

In rodents and humans, *GPR17* is expressed during development in immature non-myelinating oligodendrocytes (Chen et al., 2009; Ou et al., 2016; Satoh et al., 2017; Merten et al., 2018; Wang et al., 2020). To examine whether *gpr17* expression is comparable in zebrafish, we first analyzed its temporal expression by exon-exon junction-spanning RT-PCR in developing zebrafish. We detected *gpr17* expression during embryogenesis and early larval stages (Figure 1B), when zebrafish oligodendrocyte-lineage cells are first specified and subsequently differentiated (Kucenas et al., 2008). Consistent with this observation, RNAscope whole-mount *in situ* hybridization (WISH) analysis revealed the localization of *gpr17* mRNA from 56 h post fertilization (hpf) to 4 days post fertilization (dpf) within *olig2*$^+$ cells that were located in the dorsal part of the spinal cord of transgenic *Tg*(*olig2*:*EGFP*) zebrafish (Figures 1C–1E). *olig2* is a specific marker for oligodendrocyte-lineage cells, present during their progression from oligodendrocyte precursor cells (OPCs), which migrate toward their dorsally located target axon, to pre-myelinating and myelinating oligodendrocytes (Buckley et al., 2010; Ackerman and Monk, 2016). Notably, in contrast to 56 hpf (Figure 1C), at which all dorsal *olig2*$^+$ cells expressed *gpr17*, at 3 and 4 dpf, when oligodendrocyte myelination begins (Preston and Macklin, 2015; Ackerman and Monk, 2016), dorsal *olig2*$^+$ cells that did not express *gpr17* were also detected (Figures 1D and 1E). These data suggested that *gpr17* might not be expressed in more differentiated oligodendroglial cells. To test our hypothesis, we performed additional RNAscope WISH analyses in the transgenic line *Tg*(*claudinK*:*EGFP*), which specifically labels differentiated oligodendrocytes in early stages of myelin formation (Münzel et al., 2012). No *gpr17* mRNA was detected within *claudinK*$^+$ cells in the dorsal area of the spinal cord at 3 dpf (Figure 1F). Likewise, *gpr17* was also absent in *mbp*$^+$ cells located in the

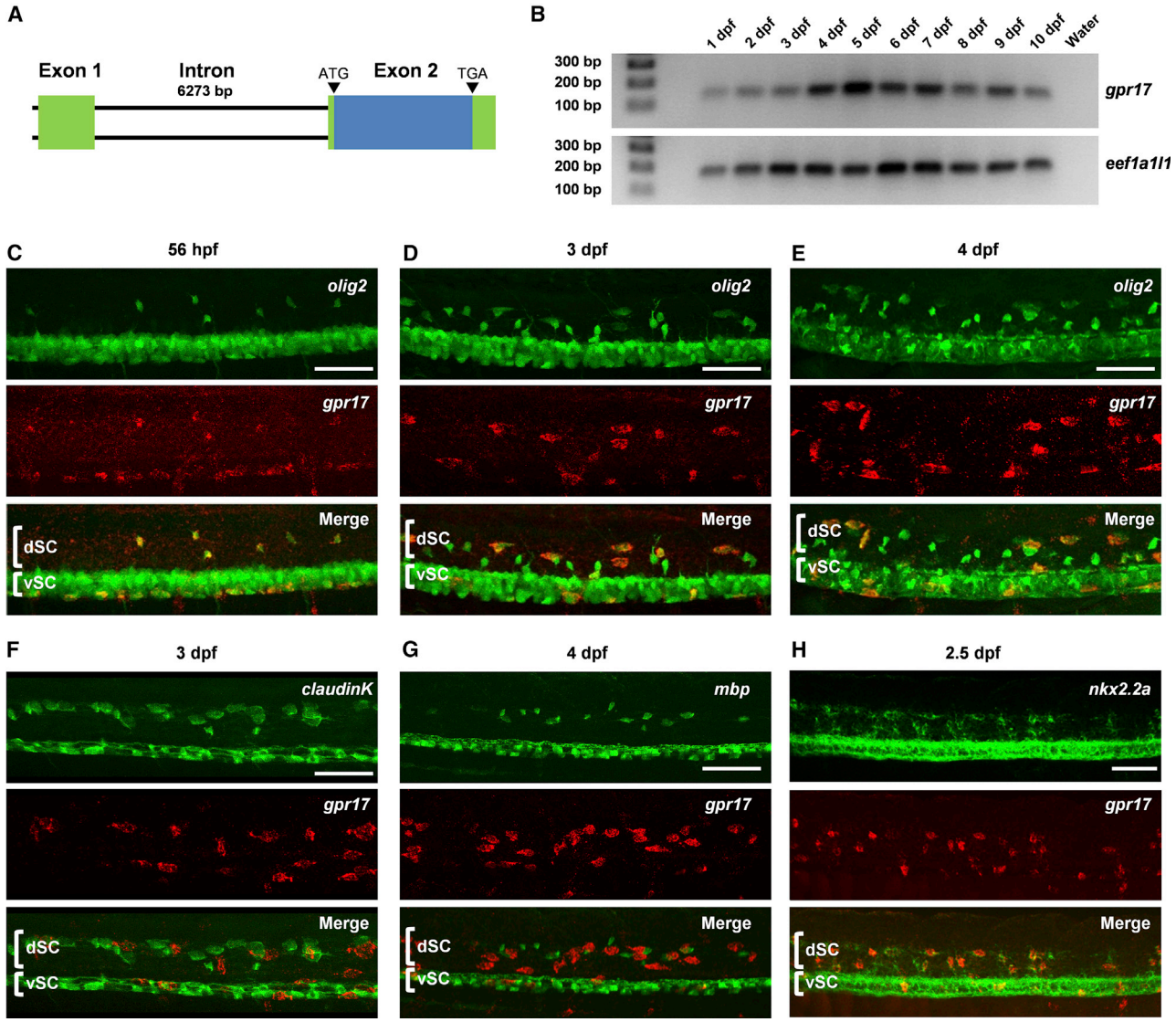


**Figure 1. Expression of *gpr17* during oligodendrocyte development**

(A) Schematic showing the zebrafish *gpr17* gene, consisting of two exons (green boxes) separated by an intron. The open reading frame (blue) is located in the second exon.

(B) Representative gel image of *gpr17* expression assessed by RT-PCR through larval development, with translation elongation factor 1-alpha *eef1a1l1* as positive control. Whole larvae were used to prepare RNA at different days post fertilization (dpf).

(C–H) Representative lateral fluorescence images of RNAscope analyses of *gpr17* (red) in spinal cords of larvae expressing *Tg*(*olig2*:*EGFP*) from 56 hpf to 4 dpf (C–E), *Tg*(*claudinK*:*EGFP*) at 3 dpf (F), *Tg*(*mbp*:*EGFP*) at 4 dpf (G), and *Tg*(*nkx2.2a*:*mEGFP*) at 2.5 dpf (H). Brackets mark the dorsal (dSC) and ventral (vSC) spinal cord; anterior is to the left, dorsal is up. Scale bars: 50 μm. See also Figures S1 and S2.

dorsal spinal cord of the transgenic reporter of mature myelinating oligodendrocytes *Tg*(*mbp*:*EGFP*) (Jung et al., 2010) at 4 dpf (Figure 1G). We concluded that terminally differentiating oligodendrocytes do not express *gpr17*.

To further assess *gpr17* expression, we used the *Tg*(*nkx2.2a*:*mEGFP*) transgenic reporter, which labels membranes of premyelinating oligodendrocytes that extend long-membrane processes to ensheathe axons but do not yet initiate the formation of myelin (Kirby et al., 2006; Ackerman et al., 2015; Ackerman and Monk, 2016). We found robust localization of *gpr17* mRNA within *nkx2.2a*$^{+}$ cells in the dorsal part of transgenic zebrafish spinal cords at 2.5 dpf (Figure 1H), when OPCs transition into pre-myelinating oligodendrocytes (Takada and Appel, 2010; Ackerman and Monk, 2016). Altogether, our data reveal that in zebrafish *gpr17* is expressed in the oligodendrocyte lineage in a developmentally regulated manner, with expression being downregulated when oligodendrocytes begin their terminal maturation. These findings are congruent with the temporal expression profile observed in mouse and human oligodendroglial cells (Chen et al., 2009; Satoh et al., 2017) and support the notion that *GPR17* expression is conserved from zebrafish to mammals.

### *gpr17* modulates oligodendrocyte differentiation in zebrafish

To investigate whether Gpr17 function is also conserved in zebrafish, we used CRISPR-Cas-9 technology to generate a *gpr17* germline mutation. We designed a single guide RNA (sgRNA) to target *gpr17* exon 2 within the coding sequence. Upon genome editing, we identified a 43-bp deletion within the coding sequence of the *gpr17* gene and refer to this mutant hereafter as *gpr17-Δ43* (Figure 2A). *Gpr17-Δ43* is characterized by a frameshift mutation leading to a premature stop codon and, in consequence, a severely truncated protein (Figures 2B and S3). Because the *gpr17* mutant allele lacks the intracellular loop 2; the transmembrane domains 4–7, including their connecting extracellular and intracellular loops; as well as the entire C-terminal cytoplasmic tail, we considered the *gpr17-Δ43* fish as a *gpr17* null mutant.

*Gpr17-Δ43* zebrafish were viable, produced viable offspring, and did not show any morphological defects compared with wild-type (WT) siblings (Figure 2C), congruent with observations in $Gpr17^{-/-}$ mice (Chen et al., 2009). To investigate whether oligodendrocyte differentiation is also accelerated in *gpr17-Δ43* zebrafish as reported for *Gpr17*-deficient mice (Chen et al., 2009), they were crossed with the transgenic reporter line *Tg*(*nkx2.2a*:*mEGFP*) or *Tg*(*mbp*:*EGFP*). We found augmented *nkx2.2a* expression in the ventral track of the spinal cord in *gpr17-Δ43* larvae at 56 hpf compared with WT fish (Figures 2D and 2E), suggestive of an increased presence of pre-myelinating oligodendrocytes in this region of the mutant fish. Indeed, analyses in *Tg*(*mbp*:*EGFP*) larvae revealed that, in contrast to WT, $mbp^{+}$ oligodendrocyte cell bodies were already detectable in the *gpr17-Δ43* ventral spinal cord at 2.5 dpf (Figure 2F), a larval stage in which axons are not yet myelinated in WT fish (Buckley et al., 2010). Moreover, the number of $mbp^{+}$ cells located in the ventral tract of the spinal cord at 3 dpf, when myelination commences around ventral axons (Buckley et al., 2010; Koudelka et al., 2016; Karttunen et al., 2017), was increased in mutant larvae (Figures 2G and 2H). Immunostaining in spinal cord sections against the proliferating cell nuclear antigen (Pcna) (Herce et al., 2014; Nagarajan et al., 2020) showed no variations in *gpr17-Δ43* compared with WT (Figure 2I), suggesting no changes in cell proliferation rates that could account for $mbp^{+}$ augmentation. Notably, despite the early onset of *mbp* expression in *gpr17-Δ43* fish, differentiation into oligodendrocytes over time eventually reached the same $mbp^{+}$ cell number as in WT at 4 dpf (Figure 2J), a finding in line with earlier observations reported in $Gpr17^{-/-}$ mice (Chen et al., 2009).

Collectively, our data suggest that, in *gpr17-Δ43*, differentiation into $mbp^{+}$ mature oligodendrocytes proceeds earlier than in WT fish. Therefore, we concluded that *gpr17-Δ43* displays a phenotype similar to that previously described for *Gpr17*-deficient mice (Chen et al., 2009; Ou et al., 2016).

### *gpr17* inactivation affects dorsal oligodendroglial cell migration in zebrafish

To further examine the role of *gpr17* in zebrafish oligodendrocyte biology, we also analyzed the effect of *gpr17* inactivation on migration of oligodendrocyte precursors. To visualize OPC migration, we used the transgenic reporter line *Tg*(*olig2*:*EGFP*) and quantified the $olig2^{+}$ cells that occupied the dorsal spinal cord at 56 hpf, when OPCs are migrating away from the primary motoneuron (pMN) domain toward dorsally located target axons (Buckley et al., 2010; Takada and Appel, 2010). We observed a reduced number of dorsal $olig2^{+}$ cells in *gpr17-Δ43* larvae compared with WT controls (Figures 3A and 3B). Congruent with this finding, the number of dorsally located $claudinK^{+}$ cells in *gpr17-Δ43*;*Tg*(*claudinK*:*EGFP*) larvae at 3 dpf (Figures 3C and 3D) and the number of dorsal $mbp^{+}$ cells in *gpr17-Δ43*;*Tg*(*mbp*:*EGFP*) larvae at 4 dpf (Figures 3E and 3F) were also reduced compared with WT fish. We observed that, over time, dorsal $mbp^{+}$ cells in *gpr17-Δ43* eventually reached the same level as WT at 5 dpf (Figures 3G and 3H), thus displaying a delay in the appearance of myelinating oligodendrocytes at their target axons in the dorsal area of the spinal cord.

This decrease in cell numbers was not due to augmented cell death because immunostaining analysis using cleaved caspase 3 antibody (Jänicke et al., 1998; Nagarajan et al., 2020) showed no increase in apoptotic cells within the spinal cord (Figure 3I). Furthermore, immunostaining analyses to detect acetylated tubulin (Figure 3J), which marks axons (Takada and Appel, 2010), and synaptic vesicle protein 2 (Sv2) (Figure 3K), which labels axonal presynaptic innervation (Wan et al., 2010), were comparable between *gpr17-Δ43* and WT larvae, indicating no defects in neuronal development that could impair oligodendrocyte development. Finally, to test the possibility of off-target CRISPR effects that could cause the observed phenotype in the mutant fish, we performed mRNA rescue experiments by injecting *zf-gpr17* mRNA into *gpr17-Δ43*;*Tg*(*olig2*:*EGFP*) embryos at the one-cell stage. Quantification of the dorsal $olig2^{+}$ cells revealed reversal of the mutant phenotype when *zf-gpr17* mRNA was injected, in contrast to injections with control *tdTomato* *m*RNA (Figures 3L, 3M, and S4). Therefore, our rescue experiments support a direct relationship between inactivation of *gpr17* and the phenotype observed in this mutant zebrafish larva.

To further support our findings with an alternative genetic strategy, we knocked down *gpr17* using an antisense translation blocking Morpholino oligonucleotide (MO). Larvae injected with *gpr17* MO did not present alterations in animal size or general development (Figure S5A), increase in the expression of cleaved caspase 3 (Figure S5B), or overt defects in the development of neurons (Figures S5C and S5D) compared with control Morpholino (CoMO)-injected larvae, ruling out unspecific effects of *gpr17* MO injection on cell survival and proliferation. In contrast, quantification of migrated oligodendroglial cells in *Tg*(*olig2*:*EGFP*) larvae injected with MO showed significantly fewer dorsally located $olig2^{+}$ cells compared with uninjected and CoMO-injected larvae (Figures S5E and S5F). We also found a reduction in the numbers of dorsal $claudinK^{+}$ cells in *Tg*(*claudinK*:*EGFP*) larvae (Figures S5G and S5H) and $mbp^{+}$ cells in the *Tg*(*mbp*:*EGFP*) larvae (Figures S5I and S5J). mRNA rescue experiments comprising co-injecting the *gpr17* MO together with *zf-gpr17* mRNA into *Tg*(*olig2*:*EGFP*) embryos revealed a reversal of the MO phenotype (Figures S5K and S5L). Therefore, knockdown of *gpr17* by MO recapitulated the phenotype observed in *gpr17-Δ43* larvae, thus corroborating our previous findings in the mutant fish.

Collectively, our data suggest a model in which inactivation of *gpr17* leads to acceleration of the cellular program that drives oligodendrocyte-lineage cell differentiation, resulting in early

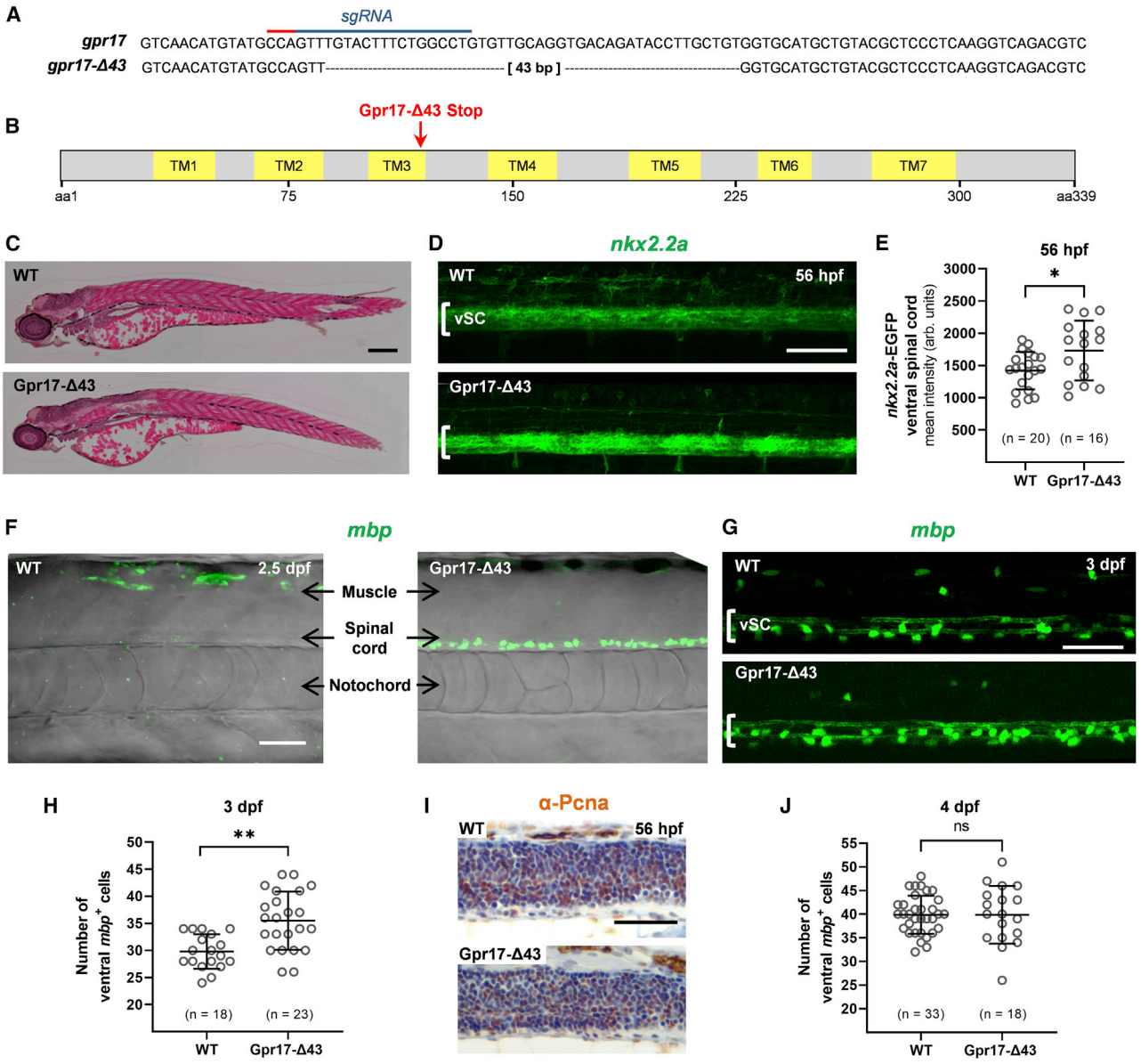


**Figure 2. *gpr17* modulates oligodendrocyte differentiation in zebrafish**

(A) *gpr17* WT and germline CRISPR mutant *gpr17-Δ43* DNA sequences; the sgRNA target (blue) and PAM site (red) are shown on the WT sequence; dashes indicate nucleotide deletions.

(B) Diagram of the Gpr17 protein (transmembrane domains are boxed in yellow) with location of the early stop caused by nucleotide deletion in the mutant fish.

(C) Hematoxylin and eosin staining images of WT and *gpr17-Δ43* siblings at 4 dpf; scale bar: 300 μm.

(D) Illustrative lateral view of spinal segments of WT and *gpr17-Δ43* larvae expressing *Tg*(*nkx2.2a*:*mEGFP*) at 56 hpf.

(E) Mean fluorescence intensity from average projections acquired from z stacks of WT and *gpr17-Δ43* ventral spinal cords expressing *Tg*(*nkx2.2a*:*mEGFP*).

(F) Representative merged bright-field and fluorescence images showing lateral views of WT and *gpr17-Δ43* larvae carrying the *Tg*(*mbp*:*EGFP*) reporter at 2.5 dpf.

(G and H) Illustrative images depicting lateral view of the spinal cords (G), and quantification of ventral spinal cord *mbp*$^+$ cells (H), of WT and *gpr17-Δ43* larvae at 3 dpf.

(I) Illustrative images of comparable sagittal paraffin sections of WT and *gpr17-Δ43* larvae at 56 hpf showing proliferating cells within the spinal cord labeled with anti-Pcna (brown staining); sections were counterstained with hematoxylin.

(J) Quantification of ventral spinal cord *mbp*$^+$ cells in WT and *gpr17-Δ43* larvae expressing *Tg*(*mbp*:*EGFP*) at 4 dpf. Brackets mark the ventral spinal cord (vSC) in (D) and (G); anterior is to the left, dorsal is up. Scale bars (except in C): 50 μm. Error bars represent mean values ± SD. *$p < 0.05$; **$p < 0.01$; ns, not significant. Two-tailed unpaired t test; n, number of fish larvae analyzed. See also Figure S3.

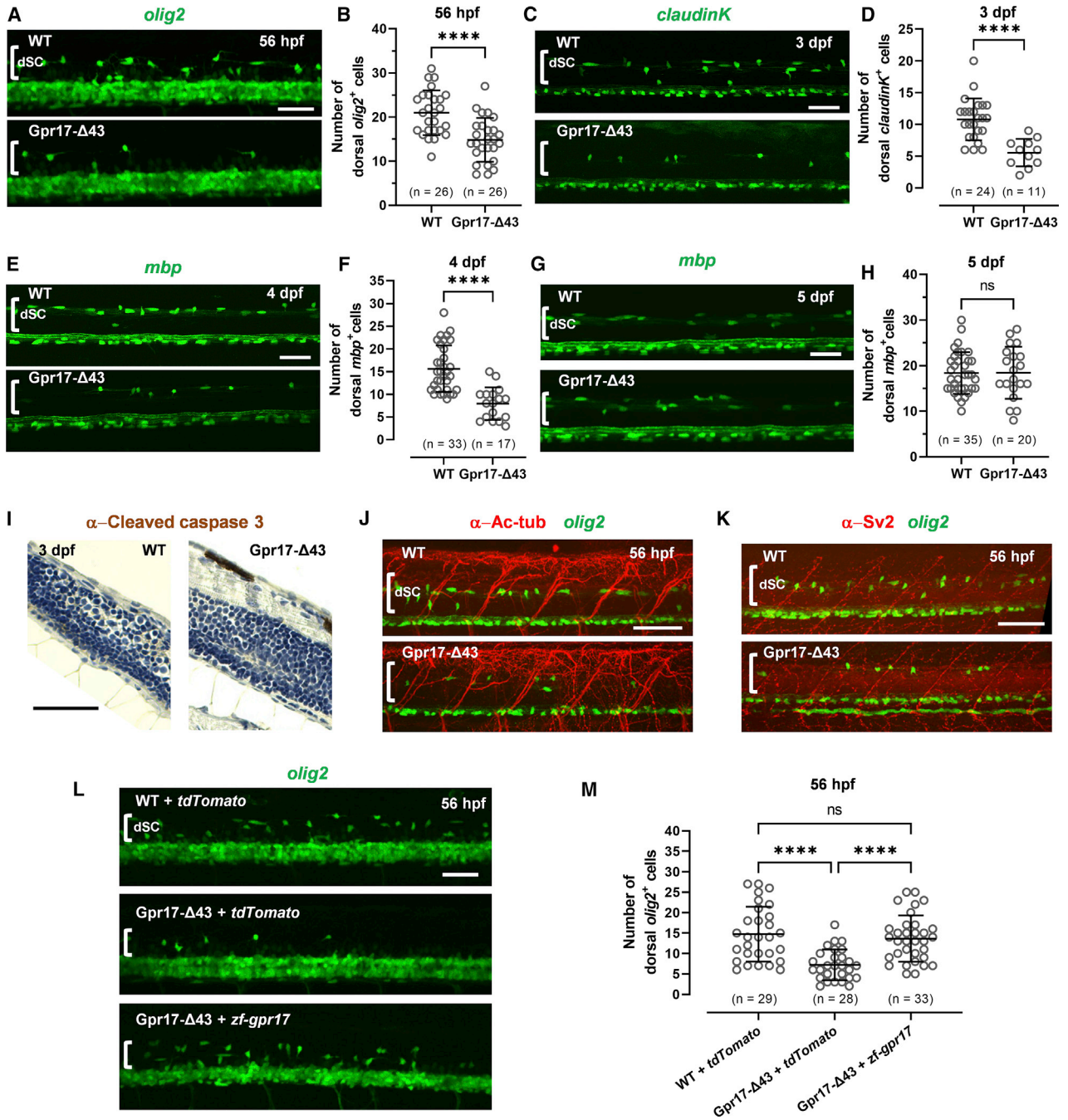


**Figure 3. *gpr17* affects dorsal oligodendroglial cell migration in zebrafish**

(A–H) Representative images depicting lateral view of the spinal cord (A, C, E, and G), as well as quantification of dorsal positively labeled cells (B, D, F, and H), in WT and *gpr17-Δ43* larvae expressing *Tg*(*olig2*:*EGFP*) at 56 hpf (A and B), *Tg*(*claudinK*:*EGFP*) at 3 dpf (C and D), and *Tg*(*mbp*:*EGFP*) at 4 dpf (E and F) and 5 dpf (G and H).

(I) Illustrative images of comparable sagittal views of paraffin sections of 3 dpf larvae labeled with anti-cleaved caspase 3 (brown staining) to recognize apoptotic cells within the spinal cord; sections were counterstained with hematoxylin.

(J and K) Representative spinal cord whole-mount immunohistochemical stainings with anti-acetylated tubulin antibody (red) to label axons (J) and anti-Sv2 antibody (red) to mark presynaptic terminals (K) in WT and *gpr17-Δ43* larvae carrying the *Tg*(*olig2*:*EGFP*) reporter (green) at 56 hpf.

(L and M) Illustrative images depicting lateral views of the spinal cord (L), as well as quantification of dorsal *olig2*$^+$ cells (M), in WT and *gpr17-Δ43* larvae of *Tg*(*olig2*:*EGFP*) at 56 hpf upon injection of *tdTomato* (as injection control) or *zf-gpr17* mRNAs. Brackets in fluorescence images mark the dorsal spinal cord (dSC); anterior is to the left, dorsal is up. Scale bars: 50 μm. Error bars represent mean values ± SD; ****$p < 0.0001$; ns, not significant. Two-tailed unpaired t test (B, D, F, and H); one-way ANOVA with Tukey's *post hoc* test (M); n, number of fish larvae analyzed. See also Figures S4 and S5.

onset of oligodendrocyte maturation and deficiency in the ability to migrate to their normal destinations. This model also explains the delayed appearance of myelinating oligodendrocytes at their target axons in the dorsal area of the spinal cord. Overall, our findings support the notion that Gpr17 is a negative regulator of oligodendrocyte differentiation in zebrafish and point to a conserved functional role of this receptor from zebrafish to mammals.

### Zebrafish Gpr17 is unresponsive to the small-molecule GPR17 agonist MDL29,951

Identification of compounds that inhibit GPR17 to stimulate myelin regeneration is a promising strategy for the treatment of human demyelinating diseases (Merten et al., 2018; Dziedzic et al., 2020). We wanted to exploit zebrafish as a model system that would allow us to search for such compounds. However, zf-Gpr17 shares an amino acid identity of only 56% with human GPR17 (h-GPR17), which raises the question of whether ligands that can bind to h-GPR17 are also capable of interacting with zf-Gpr17. To clarify this question, we generated mammalian human embryonic kidney (HEK) 293 cell lines recombinantly expressing both receptor orthologs. ELISA (Figure 4A) and immunocytochemical staining (Figure 4B) confirmed proper plasma membrane localization of zf-Gpr17 and h-GPR17 in this cellular background. However, analysis of receptor function using label-free whole-cell biosensing based on dynamic mass redistribution (DMR), a technology platform that portrays GPCR signaling along all four major G protein pathways (Schröder et al., 2010, 2011), revealed a striking difference: unlike h-GPR17 HEK293 cells, which responded with robust and concentration-dependent changes to treatment with MDL29,951, a synthetic small-molecule GPR17 agonist (Hennen et al., 2013), zf-Gpr17-HEK293 cells were unresponsive, just like pcDNA3.1 vector-transfected control cells (Figure 4C). Apparently MDL29,951, known to specifically activate h-GPR17 in heterologous cell expression systems (Figure 4C) (Hennen et al., 2013; Simon et al., 2017; Baqi et al., 2018; Conley et al., 2021) as well as in rodent oligodendrocyte cultures (Ou et al., 2016; Simon et al., 2016), is no suitable chemical activator for zf-Gpr17. To distinguish whether inactivity of zf-Gpr17 arose from deficient ligand recognition as opposed to deficient interaction of the fish ortholog with the mammalian HEK293 signaling machinery, we designed and created chimeric receptors, combining the extracellular and transmembrane segments of h-GPR17 with the intracellular loops and the C-terminal tail of zf-Gpr17 (h/zf-GPR17) and vice versa (zf/h-Gpr17) (Figure 4D). Indeed, while both receptor chimeras were expressed at the cell surface (Figure 4E), albeit at lower abundance compared with their WT counterparts (Figure 4F), only h/zf-GPR17, and not the reverse chimera zf/h-Gpr17, was sensitive to stimulation with MDL29,951 (Figures 4G and 4H). These data led us to conclude that the unresponsiveness of zf-Gpr17 to MDL29,951 most likely originates from insufficient homology within the putative ligand binding site, which precludes efficient interaction of MDL29,951 with the zebrafish ortholog.

### *h-* and *h/zf-GPR17* mRNAs rescued *gpr17*-deficient larval phenotypes

The inactivity of MDL29,951 on zf-Gpr17 calls into question the use of zebrafish as an *in vivo* animal model to analyze novel compounds with pro-myelination effects in humans. We hypothesized that humanizing zebrafish via expression of the h-GPR17 in fish larvae could circumvent this issue, provided that zebrafish and human GPR17 are functionally equivalent. We injected *h-GPR17* and *h/zf-GPR17* mRNAs into *gpr17-Δ43*;*Tg*(*olig2*:*EGFP*) embryos at the one-cell stage and analyzed the occurrence of a rescue effect similar to that observed with *zf-gpr17* mRNA (Figure 3M). Indeed, injection with either *h-GPR17* or *h/zf-GPR17* mRNAs completely recovered the number of dorsal *olig2*$^+$ cells in *gpr17-Δ43* compared with WT fish (Figures 5A and 5B). Likewise, the enhanced number of ventrally located *mbp*$^+$ cells observed in *gpr17-Δ43*;*Tg*(*mbp*:*EGFP*) embryos at 3 dpf was significantly diminished upon these mRNA injections, essentially restoring the WT phenotype (Figures 5C and 5D). The ability of *h-* and *h/zf-GPR17* mRNAs to rescue the *gpr17*-deficient larval phenotype proved the effective functionality of the injected receptors and revealed the ability of human GPR17 to efficiently replace the zebrafish ortholog in the *in vivo* context. Moreover, these data again strengthened the notion that the phenotype observed in *gpr17-Δ43* fish was caused by specific and efficient inactivation of zebrafish Gpr17.

### Small-molecule synthetic antagonist UCB6651 dampens GPR17 signaling *in vitro* with high potency and selectivity

To evaluate the extrapolative capabilities of the *GPR17*-humanized zebrafish for analysis of potential pro-myelinating compounds acting via targeted inhibition of h-GPR17, we took advantage of the GPR17 antagonist UCB6651 (Figures 6A and S6), developed to inhibit GPR17 with high potency and selectivity (compound I-255 in Müller et al., 2018). UCB6651 efficiently countered MDL29,951-mediated inhibition of cAMP formation (Figure 6B), mobilization of intracellular $Ca^{2+}$ from endoplasmic reticulum stores (Figure 6C), and cell morphological changes determined with DMR biosensing (Figure 6D) in the nanomolar potency range. An additional challenge in GPCR ligand discovery is identification of molecules with specificity for the target receptor. GPR17 is phylogenetically intermediate between the purinergic P2RY and the cysteinyl leukotriene (CYSLT) receptors (Figure 6E). Therefore, we determined the selectivity of UCB6651 for GPR17 over five phylogenetically related receptor neighbors. At concentrations exceeding its $pIC_{50}$ by a factor of ~1,000, UCB6651 totally blunted signaling of GPR17 (Figure 6F) but was completely inert on ligand-activated P2RY receptors as well as on the CYSLT receptor subtype 1 (Figures 6G and 6H). Consistent with high selectivity for GPR17 inhibition, UCB6651 also promoted maturation of primary rat oligodendrocytes endogenously expressing GPR17, as evident from enhanced MBP expression (Figure 6I). This *in vitro* profile led us to conclude that UCB6651 may be well suited to probe the contribution of GPR17 in developing humanized zebrafish larvae *in vivo*.

### *GPR17*-humanized zebrafish as proof of principle for *in vivo* analysis of potential pro-myelinating compounds acting as blockers of GPR17

To examine whether UCB6651 affects oligodendrocyte lineage progression in zebrafish larvae, we injected *h-GPR17* mRNA

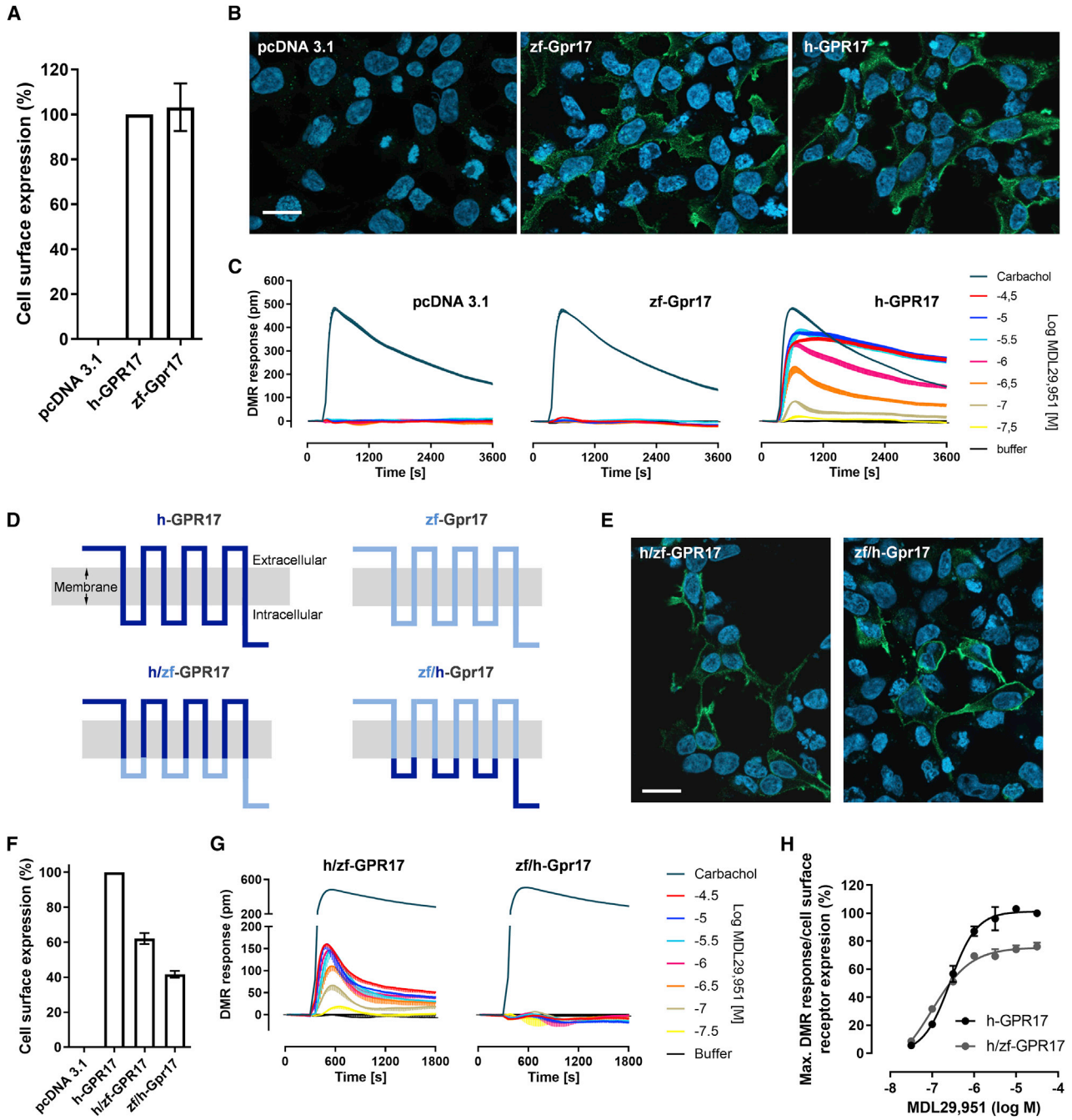


**Figure 4. Zebrafish Gpr17 is unresponsive to MDL29,951**

(A) Normalized ELISA quantification of cell-surface h-GPR17 (set to 100%), zf-Gpr17, and vector (pcDNA 3.1) in transfected HEK293 cells.

(B) Representative fluorescence images of vector, zf-Gpr17, and h-GPR17 in transfected HEK293 cells.

(C) Representative traces of MDL29,951 determined by label-free DMR assays in HEK293 cells transfected with vector, zf-Gpr17, and h-GPR17.

(D) Serpentine scheme of the wild-type and chimeric receptors constructed and analyzed in this study.

(E) Representative images showing immunofluorescence detection of the chimeric receptors h/zf-GPR17 and zf/h-Gpr17 expressed in HEK293 cells.

(F) Normalized ELISA quantification of cell-surface h-GPR17 (set to 100%) and chimeric receptors.

(G) Representative time-course traces of whole-cell DMR recorded in HEK293 cells transiently transfected with the indicated receptors and treated with different concentrations of MDL29,951.

(H) Comparison of GPR17 function triggered by different concentrations of MDL29,951 and corrected for relative cellular abundance for each transfected receptor construct. Data are presented as percentage of 31.6 μM MDL29,951 (set to 100%). Scale bars: 20 μm. Label-free signatures are shown as representative traces (mean + SEM), measured in triplicate; carbachol (100 μM) activation of cell endogenous muscarinic receptors was included as a viability control. Error bars represent mean values ± SEM. Experiments were independently repeated three times.

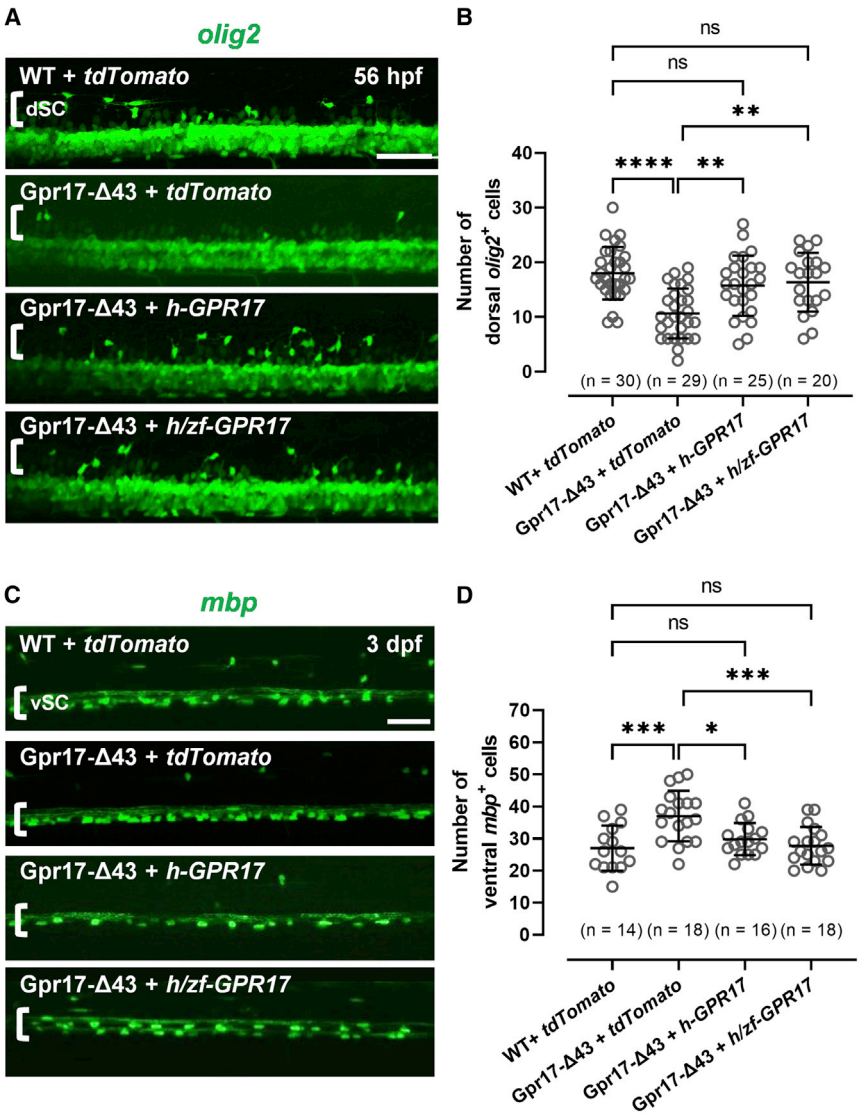


**Figure 5. *h-* and *h/zf-GPR17* mRNAs rescued the phenotype observed in *gpr17*-deficient larvae**

(A and B) Representative images depicting lateral views of the spinal cord (A), as well as quantification of dorsal *olig2*$^+$ cells (B), in WT and *gpr17-Δ43* larvae of *Tg*(*olig2*:*EGFP*) at 56 hpf upon injection of *tdTomato* (as injection control), *h-GPR17*, or *h/zf-GPR17* mRNAs.

(C and D) Illustrative images showing lateral views of the spinal cords (C), and quantification of ventral spinal cord *mbp*$^+$ cells at 3 dpf (D), of WT and *gpr17-Δ43* larvae carrying the *Tg*(*mbp*:*EGFP*) reporter upon injection of *tdTomato*, *h-GPR17*, or *h/zf-GPR17* mRNAs. Brackets in images mark the dorsal (dSC; [A]) and ventral (vSC; [C]) spinal cords; scale bars: 50 μm. Error bars represent mean values ± SD; *p < 0.05, **p < 0.01, ***p < 0.001, ****p < 0.0001; ns, not significant. One-way ANOVA with Tukey's *post hoc* test; n, number of fish larvae analyzed.

into *gpr17-Δ43*;*Tg*(*olig2*:*EGFP*) embryos at the one-cell stage and exposed the dechorionated larvae to either UCB6651 or solvent. Treatment with UCB6651 but not with solvent control decreased the number of dorsal *olig2*$^+$cells in *GPR17*-humanized larvae, indicating a counteracting functional effect of UCB6651 on GPR17, but also that pharmacological inhibition of h-GPR17 phenocopies the effect of genetic deletion (Figures 7A and 7B). Conversely, no reduction in dorsal *olig2*$^+$ cell numbers was apparent after treatment with UCB6651 in *gpr17-Δ43*;*Tg*(*olig2*:*EGFP*) larvae injected with *zf-gpr17* mRNA (Figures 7C and 7D), suggesting specific interaction of the GPR17 blocker with the human but not the zebrafish ortholog. In line with this finding, UCB6651 reduction of dorsal *olig2*$^+$ cells was restored when *gpr17-Δ43*;*Tg*(*olig2*:*EGFP*) embryos were injected with *h/zf-GPR17* mRNA (Figures 7E and 7F). Therefore, our data support the specific interaction of UCB6651 with GPR17 harboring the human, but not the zebrafish, extracellular face of the receptor. To further corroborate our findings, we also injected *h-GPR17* mRNA into *gpr17-Δ43*;*Tg*(*mbp*:*EGFP*) embryos, and assessed the number of *mbp*$^+$ cells in the ventral spinal cord upon treatment with UCB6651 at 3 dpf. As expected, UCB6651, but not the solvent control or the inactive analog EMI280422 (Figures 7G, 7H, and S7), increased ventral *mbp*$^+$ cell numbers in *GPR17*-humanized larvae, comparable in extent to *gpr17-Δ43*;*Tg*(*mbp*:*EGFP*) embryos injected with *tdTomato* *m*RNA instead of *h-GPR17* mRNA (Figures 7I and 7J).

Taken together, our data provide strong support for the notion that human and zebrafish Gpr17s are functionally interchangeable and that UCB6651 effectively inhibits only h-GPR17 when expressed in the zebrafish, arguing that our humanized zebrafish is both suitable and prerequisite for further *in vivo* analysis of pro-myelinating compounds acting via targeted inhibition of h-GPR17.

## DISCUSSION

Drug discovery and biomedical research rely heavily on animal models to understand human disease pathology in cellular and molecular detail and to provide *in vivo* systems for developing and testing new therapeutic modalities. In our study, we introduce a humanized zebrafish as proof of principle to aid in the search for pharmacological agents that promote the regenerative process of remyelination via specific inhibition of GPR17. Unlike the remaining treatment options for demyelinating diseases such as MS, which target immune functions to reduce CNS inflammation, inhibition of GPR17 would promote neuroprotection and axonal survival by enhancing CNS myelin regeneration. In fact, the discovery of novel drugs that promote acquisition of new myelin sheaths has become an important strategy for the treatment of MS.

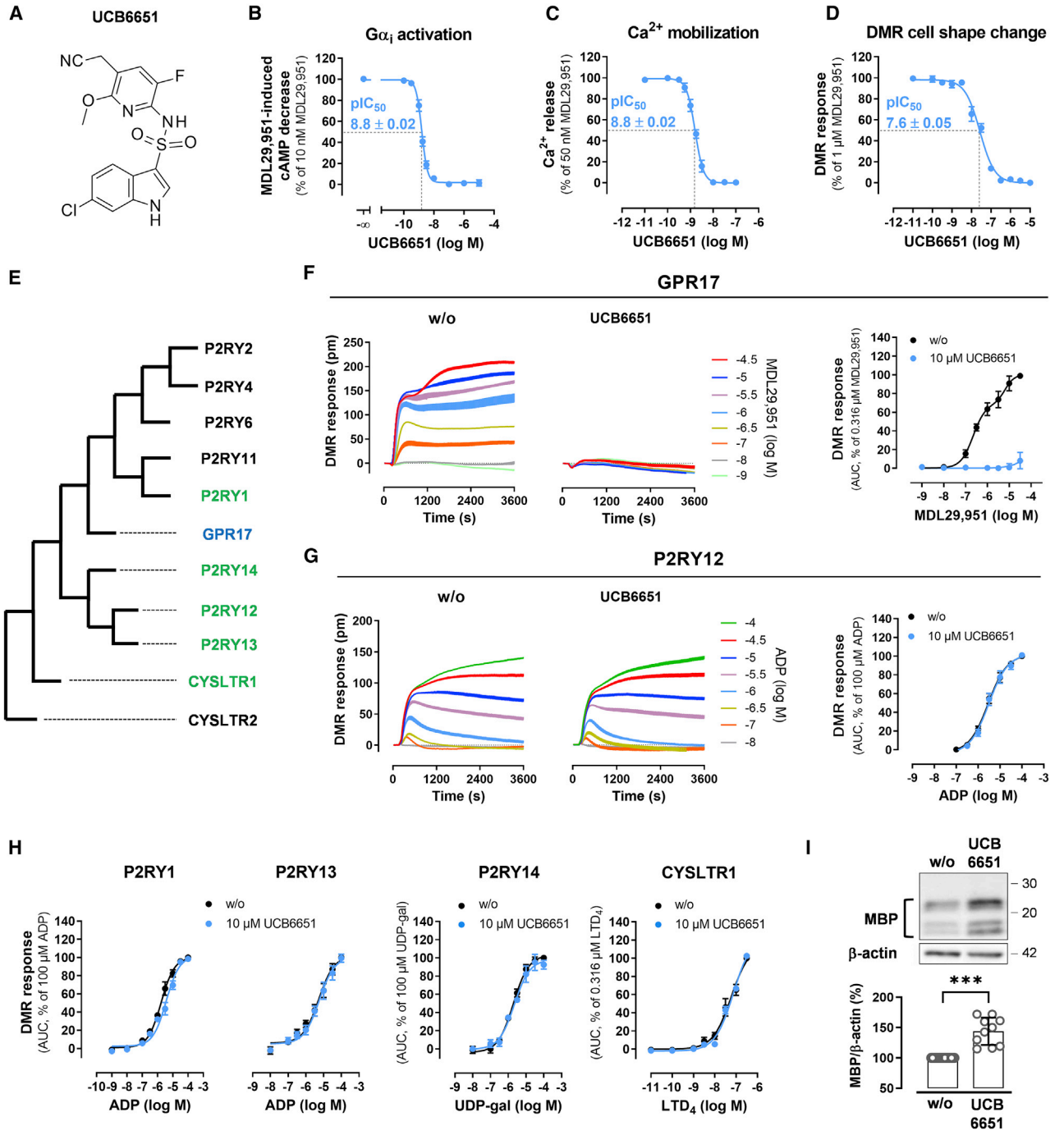


**Figure 6. Small-molecule synthetic antagonist UCB6651 dampens GPR17 signaling *in vitro* with high potency and selectivity**

(A) Chemical structure of UCB6651.

(B–D) Normalized concentration-dependent inhibition curves of UCB6651 on h-GPR17-mediated cAMP decrease quantified as inhibition of MDL-mediated cAMP lowering of forskolin-stimulated adenylyl cyclase (B), calcium mobilization (C), and DMR cell shape change (D) induced with MDL29,951 at its $EC_{80}$/$EC_{90}$ in CHO cells stably transfected with h-GPR17.

(E) Phylogenetic tree showing the relationship between GPR17 and P2RY and CYSLT receptors.

(F) Representative concentration-dependent activation traces of MDL29,951-stimulated h-GPR17 in the absence (w/o) or presence of 10 µM UCB6651 as determined by label-free DMR biosensing in CHO-GPR17 cells and corresponding normalized concentration effect curves.

(G) Representative traces of ADP-triggered whole-cell DMR responses in 1321N1 cells stably expressing P2RY12 and pre-treated without (w/o) or with 10 µM UCB6651 (left and middle), and normalized averaged concentration-effect curves (right).

(H) Effects of 10 µM UCB6651 on ligand-mediated whole-cell activation of receptors closely related to GPR17 and measured in stable P2RY1-1321N1, P2RY13-1321N1, P2RY14-HEK293, and CYSLTR1-HEK293 cells.

*(legend continued on next page)*

Zebrafish (*D. rerio*) has evolved into a valuable vertebrate model to recapitulate oligodendrocyte biology and myelination in the *in vivo* setting (Preston and Macklin, 2015; Ackerman and Monk, 2016; Czopka, 2016). As a vertebrate, it has intact organs comparable to mammals, conserving molecular and cellular functions (Chen et al., 2020). Notably, during their juvenile stages, zebrafish are well suited to screening and imaging approaches because of (1) their transparency, which makes them ideal for observing cell development in real time; (2) their small body size, which is suited to fit into 96-well plates; and (3) their permeability to and absorption of small molecules through their skin following direct addition to the water (Taylor et al., 2010). Importantly, new genetic engineering techniques allow zebrafish to be genetically modified (Cornet et al., 2018). This enables manipulation of protein targets hypothesized to foster OPC differentiation and maturation in demyelinating diseases. One such protein target is GPR17, which acts as an inhibitor of oligodendrocyte maturation during postnatal development, orchestrating the transition between immature and mature myelinating oligodendrocytes (Chen et al., 2009; Merten et al., 2018). Because *GPR17* expression is highly abundant in active white matter plaques of MS patients (Chen et al., 2009), upregulation of GPR17 in demyelinating lesions might be causally responsible for remyelination arrest.

Herein, we evaluated the extrapolative capabilities of zebrafish to analyze compounds that would promote oligodendrocyte differentiation via targeted inhibition of GPR17. Our initial analyses showed that *gpr17* is expressed in zebrafish oligodendrocytes in a developmentally regulated manner akin to results previously reported for mammalian cells (Chen et al., 2009; Simon et al., 2016; Merten et al., 2018; Turan et al., 2021). Furthermore, our knockout analyses strongly suggest that Gpr17 is a negative regulator of oligodendrocyte differentiation also in zebrafish. Hence, our findings demonstrate species-conserved expression and function of GPR17 in oligodendroglial cell development, thereby minimizing potential mismatches between zebrafish and mammal oligodendroglial physiology. Nevertheless, MDL29,951, the small-molecule surrogate agonist of human and rodent GPR17 (Hennen et al., 2013; Simon et al., 2017), was inactive in cells heterologously expressing zf-Gpr17. With 56% amino acid sequence identity between the zebrafish and the human receptors, this finding may reflect the lack of conservation of the MDL29,951 binding site and/or non-conservation of the conformational changes induced by the agonist that are important for its activity. Indeed, the exchange of extracellular and transmembrane regions of zf-Gpr17 with the human receptor counterparts recovered the functionality in the chimeric receptor, clearly demonstrating the insufficient homology within the ligand binding site across species orthologs. Similar differences between zebrafish and human proteins that impair compound binding have been reported by others (Laselva et al., 2019).

Regardless, over 80% of genes that are associated with human diseases have a counterpart in zebrafish (Czopka, 2016). Thus, while sequence conservation does not justify direct drug screens in zebrafish, protein-coding sequences of zebrafish and mammals do display enough similarity to share comparable whole organism biologies as observed in this study of GPR17. This was confirmed by the ability of human GPR17 to rescue the deficient phenotype in the null mutant fish larvae, proving equivalent functionality of the human receptor in this different species. In addition, our results with UCB6651 along with an inactive analog provide proof of principle for using *GPR17*-humanized zebrafish to analyze novel compounds targeting GPR17 that potentially enhance remyelination in humans. Such an approach is expected to overcome interspecies differences that may cause drugs identified in other animal models to ultimately fail in humans. Because GPCRs belong to the most successful protein family in the history of drug development, our study may be an important step forward toward the development of a zebrafish *in vivo* platform enabling comparison of already advanced or optimized drug candidates targeting GPR17, thus more rapidly bringing benefits to patients in MS, an area of high unmet medical need.

## Limitations of the study

Our current proof-of-principle studies employed the injection of exogenous mRNA prior to compound addition. With this approach, the mRNA is globally expressed in all cell types, and there may be some animal-to-animal variability in expression levels. However, the lethality observed with enforced expression of GPR17 in mouse models (Chen et al., 2009) likely precludes generation of stable transgenic lines. Notwithstanding this caveat, mRNA injection is a viable strategy to achieve temporal expression of GPR17 without overt toxicities and would be sufficient for medium-throughput compound screens in the future.

## Significance

The discovery of therapeutic compounds to enhance myelination is highly sought after to combat demyelinating diseases such as multiple sclerosis (MS). In MS, the most prevalent disabling neurological disease among young adults worldwide, oligodendrocytes are the target of autoimmune destruction, resulting in the loss of the protective myelin sheath that encompasses neuronal axons and, ultimately, neuronal damage. All current drugs for the treatment of MS exclusively suppress immune function. However, no therapeutic agent is available to patients that enhances the number of new oligodendrocytes from their immature precursors, thus directly fostering neuronal repair. This may be, at least in part, because potentially beneficial compounds originating from phenotypic screenings and rodent MS models have a poor record of success in clinical trials, thus bringing the overall translational value of current pre-clinical analysis into question.

To bridge this translational gap, we humanized zebrafish to express the human ortholog of Gpr17, a cell-intrinsic timer and negative regulator of myelination. With humanization we can exploit the strength of this animal model for pre-clinical drug discovery, i.e., screening capabilities and whole organism biology assessment,

(I) Illustrative western blot of MBP abundance (top) and normalized quantitative analysis of MBP-immunoreactive bands corrected by β-actin (n = 10; bottom) showing that primary rat differentiating oligodendrocytes treated with UCB6651 for 48–72 h expressed higher MBP levels compared with untreated cells (set to 100%). The MBP antibody recognizes the four isoforms of MBP, which correspond to alternative transcripts of the single MBP gene. Error bars represent mean values ± SD; ***$p < 0.001$. One-sample, two-tailed t test. Label-free signatures (F and G) are shown as representative traces (mean + SEM), measured in triplicate. Normalized data (except in [I]) are presented as mean values ± SEM of at least three biologically independent experiments. See also Figure S6.

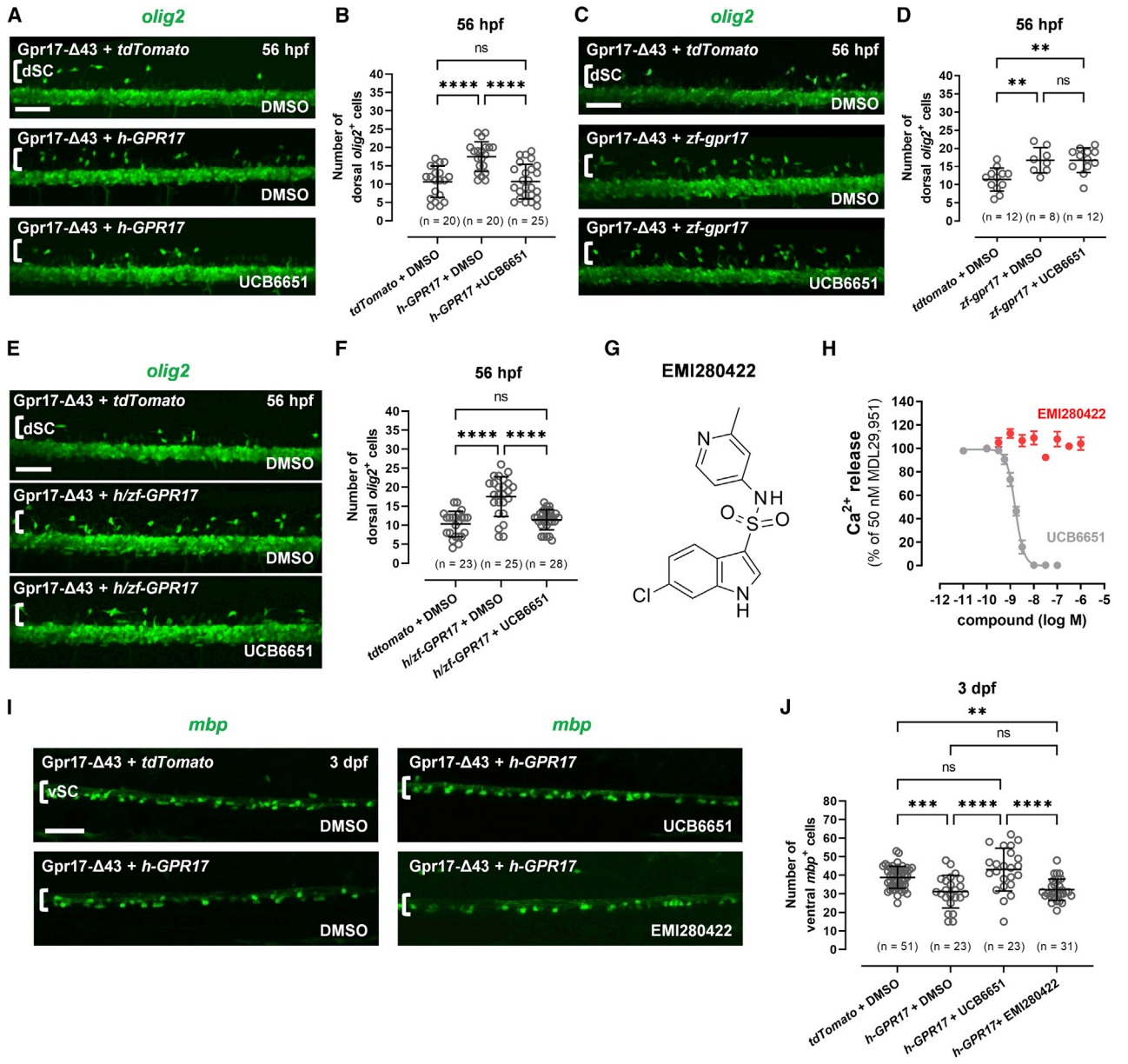


**Figure 7. *GPR17*-humanized zebrafish as proof of principle for *in vivo* analysis of potential pro-myelinating compounds acting as blockers of GPR17**

(A–F) Representative images showing lateral views of the spinal cord (A, C, and E), and quantification of dorsal *olig2*$^+$ cells (B, D, and F), in *gpr17-Δ43* larvae of *Tg*(*olig2*:*EGFP*) at 56 hpf upon injection of either *tdTomato* (as injection control) or *h-GPR17* (A and B), *zf-gpr17* (C and D), or *h/zf-GPR17* (E and F) mRNAs, and treated in the presence of solvent (DMSO) or UCB6651. Brackets in images mark the dorsal spinal cord (dSC).

(G) The structure of EMI280422.

(H) Impact of increasing concentrations of EMI280422 and UCB6651 on the MDL29,951-mediated release of intracellular calcium in CHO cells stably expressing h-GPR17. The concentration-effect curve of UCB6651 is identical to that shown in Figure 6C.

(I and J) Illustrative images showing lateral views of the spinal cords (I), and quantification of ventral spinal cord *mbp*$^+$ cells (J), at 3 dpf of *gpr17-Δ43* larvae carrying the *Tg*(*mbp*:*EGFP*) reporter upon injection of *tdTomato* or *h-GPR17* mRNAs, and treated in the absence and presence of GPR17 antagonist UCB6651 or the inactive analog EMI280422. Brackets in images mark the ventral spinal cord (vSC). Scale bars: 50 μm. Error bars represent mean values ± SD; **p < 0.01, ***p < 0.001, ****p < 0.0001; ns, not significant. One-way ANOVA with Tukey's *post hoc* test; n, number of fish larvae analyzed. See also Figure S7.

and at the same time overcome the limitations related to insufficient homology in the sites where drugs bind. Because many drugs are species specific, GPR17 humanization may be the prerequisite to enable zebrafish to report drug responses as if they were human patients. Indeed, while we provide cross-species validation of GPR17 function, a highly potent small-molecule inhibitor targeting human and rodent GPR17, but not an inactive analog, phenocopies the effects of genetic deletion only after humanization. We posit

that cross-species rescue be combined with humanization for successful implementation of zebrafish as an *in vivo* platform to truly bridge the gap between whole-cell *in vitro* and rodent models in pre-clinical drug discovery.

## STAR★METHODS

Detailed methods are provided in the online version of this paper and include the following:

- KEY RESOURCES TABLE
- RESOURCE AVAILABILITY
  - Lead contact
  - Materials availability
  - Data and code availability
- EXPERIMENTAL MODEL AND SUBJECT DETAILS
  - Zebrafish housing and maintenance
  - Cell lines
- METHOD DETAILS
  - DNA constructs
  - Enzyme-linked Immunosorbent assay (ELISA)
  - Immunocytochemistry
  - $Ca^{++}$mobilization assay
  - HTRF-based cAMP Accumulation assay
  - Label-free dynamic mass redistribution (DMR) assays
  - Western blotting
  - Rapid amplification of 5′cDNA ends (5′ RACE)
  - Exon-exon junction reverse transcription polymerase chain reaction (RT-PCR)
  - Tissue preparation and *in situ* hybridization
  - Generation of *gpr17* mutant line
  - Genotyping of the *gpr17* knockout line Δ43
  - Morpholino injections
  - mRNA injections
  - Immunohistochemistry
  - Imaging
  - Compound treatment
  - Chemical synthesis
- QUANTIFICATION AND STATISTICAL ANALYSIS

## SUPPLEMENTAL INFORMATION

Supplemental information can be found online at https://doi.org/10.1016/j.chembiol.2022.08.007.

## ACKNOWLEDGMENTS

We thank Hennig Kleinert, Öznur Yilmaz, Tobias Lindenberg, and Nina Heycke for excellent assistance; Maik Hintze for fruitful discussions; and David Lyons, Catherina G. Becker, and the European Zebrafish Resource Centre (EZRC) for transgenic fish lines. We particularly thank Erez Raz, Zahra Labbaf, and Lukasz Truszkowski for their guidance on the RNAscope assay. We are thankful for the support of the Zebrafish Core Facility (Bonn Medical Faculty). This work was supported by the Deutsche Forschungsgemeinschaft (DFG; German Research Foundation)-funded Research Training Group RTG1873 (214362475/GRK1873/2; to E.K.) and a DFG equipment grant (INST1172/37-1 FUGG) for the multiphoton microscope setup (to B.O.).

## AUTHOR CONTRIBUTIONS

Conceptualization, J.G., B.O., and E.K.; methodology, F.H., E.M., N.M., N-K.S.K., P.R., K.S., A.J., B.N., R.S., C.P., and M.G.; investigation, F.H., E.M., N.M., N-K.S.K., P.R., K.S., A.J., B.N., R.S., C.P., and M.G.; writing – original draft, E.K. and J.G.; writing – review & editing, K.R.M., B.O., E.K., and J.G., with support from all authors; visualization, F.H., N.M., and J.G.; funding acquisition, B.O. and E.K.; supervision, J.G., B.O., and E.K.

## DECLARATION OF INTERESTS

C.P. is listed as inventor on the patent WO 2018122232 A1.

Received: December 20, 2021
Revised: May 25, 2022
Accepted: August 24, 2022
Published: September 19, 2022

## REFERENCES

Ackerman, S.D., and Monk, K.R. (2016). The scales and tales of myelination: using zebrafish and mouse to study myelinating glia. Brain Res. *1641*, 79–91.

Ackerman, S.D., Garcia, C., Piao, X., Gutmann, D.H., and Monk, K.R. (2015). The adhesion GPCR Gpr56 regulates oligodendrocyte development via interactions with Gα12/13 and RhoA. Nat. Commun. *6*, 6122.

Almeida, R.G., Czopka, T., Ffrench-Constant, C., and Lyons, D.A. (2011). Individual axons regulate the myelinating potential of single oligodendrocytes *in vivo*. Development (Cambridge, England) *138*, 4443–4450.

Baker, D., and Amor, S. (2015). Mouse models of multiple sclerosis: lost in translation? Curr. Pharm. Des. *21*, 2440–2452.

Balashov, K.E. (2020). Drugs in development for multiple sclerosis. Practical Neurol. 40–43.

Balestri, S., Del Giovane, A., Sposato, C., Ferrarelli, M., and Ragnini-Wilson, A. (2021). The current challenges for drug discovery in CNS remyelination. Int. J. Mol. Sci. *22*, 2891.

Baqi, Y., Pillaiyar, T., Abdelrahman, A., Kaufmann, O., Alshaibani, S., Rafehi, M., Ghasimi, S., Akkari, R., Ritter, K., Simon, K., et al. (2018). 3-(2-Carboxyethyl)indole-2-carboxylic acid derivatives: structural requirements and properties of potent agonists of the orphan G protein-coupled receptor GPR17. J. Med. Chem. *61*, 8136–8154.

Bebo, B.F., Allegretta, M., Landsman, D., Zackowski, K.M., Brabazon, F., Kostich, W.A., Coetzee, T., Ng, A.V., Marrie, R.A., Monk, K.R., et al. (2022). Pathways to cures for multiple sclerosis: a research roadmap. Mult. Scler. *28*, 331–345.

Ben-Nun, A., Kaushansky, N., Kawakami, N., Krishnamoorthy, G., Berer, K., Liblau, R., Hohlfeld, R., and Wekerle, H. (2014). From classic to spontaneous and humanized models of multiple sclerosis: impact on understanding pathogenesis and drug development. J. Autoimmun. *54*, 33–50.

Buckley, C.E., Marguerie, A., Roach, A.G., Goldsmith, P., Fleming, A., Alderton, W.K., and Franklin, R.J.M. (2010). Drug reprofiling using zebrafish identifies novel compounds with potential pro-myelination effects. Neuropharmacology *59*, 149–159.

Chen, J., Poskanzer, K.E., Freeman, M.R., and Monk, K.R. (2020). Live-imaging of astrocyte morphogenesis and function in zebrafish neural circuits. Nat. Neurosci. *23*, 1297–1306.

Chen, Y., Wu, H., Wang, S., Koito, H., Li, J., Ye, F., Hoang, J., Escobar, S.S., Gow, A., Arnett, H.A., et al. (2009). The oligodendrocyte-specific G protein-coupled receptor GPR17 is a cell-intrinsic timer of myelination. Nat. Neurosci. *12*, 1398–1406.

Conley, J.M., Sun, H., Ayers, K.L., Zhu, H., Chen, R., Shen, M., Hall, M.D., and Ren, H. (2021). Human GPR17 missense variants identified in metabolic disease patients have distinct downstream signaling profiles. J. Biol. Chem. *297*, 100881.

Cornet, C., Di Donato, V., and Terriente, J. (2018). Combining zebrafish and CRISPR/Cas9: toward a more efficient drug discovery pipeline. Front. Pharmacol. *9*, 703.

Czopka, T. (2016). Insights into mechanisms of central nervous system myelination using zebrafish. Glia *64*, 333–349.

Dendrou, C.A., Fugger, L., and Friese, M.A. (2015). Immunopathology of multiple sclerosis. Nat. Rev. Immunol. *15*, 545–558.

Dziedzic, A., Miller, E., Saluk-Bijak, J., and Bijak, M. (2020). The GPR17 receptor-A promising goal for therapy and a potential marker of the Neurodegenerative process in multiple sclerosis. Int. J. Mol. Sci. *21*, 1852.

Early, J.J., Cole, K.L., Williamson, J.M., Swire, M., Kamadurai, H., Muskavitch, M., and Lyons, D.A. (2018). An automated high-resolution *in vivo* screen in zebrafish to identify chemical regulators of myelination. Elife *7*.

Fancy, S.P.J., Chan, J.R., Baranzini, S.E., Franklin, R.J.M., and Rowitch, D.H. (2011). Myelin regeneration: a recapitulation of development? Annu. Rev. Neurosci. *34*, 21–43.

Fields, R.D. (2008). White matter in learning, cognition and psychiatric disorders. Trends Neurosci. *31*, 361–370.

Filippi, M., Bar-Or, A., Piehl, F., Preziosa, P., Solari, A., Vukusic, S., and Rocca, M.A. (2018). Multiple sclerosis. Nat. Rev. Dis. Primers *4*, 43.

Franklin, R.J.M., and Ffrench-Constant, C. (2017). Regenerating CNS myelin - from mechanisms to experimental medicines. Nat. Rev. Neurosci. *18*, 753–769.

Friese, M.A., Montalban, X., Willcox, N., Bell, J.I., Martin, R., and Fugger, L. (2006). The value of animal models for drug development in multiple sclerosis. Brain *129*, 1940–1952.

Green, A.J., Gelfand, J.M., Cree, B.A., Bevan, C., Boscardin, W.J., Mei, F., Inman, J., Arnow, S., Devereux, M., Abounasr, A., et al. (2017). Clemastine fumarate as a remyelinating therapy for multiple sclerosis (ReBUILD): a randomised, controlled, double-blind, crossover trial. Lancet *390*, 2481–2489.

Hennen, S., Wang, H., Peters, L., Merten, N., Simon, K., Spinrath, A., Blättermann, S., Akkari, R., Schrage, R., Schröder, R., et al. (2013). Decoding signaling and function of the orphan G protein-coupled receptor GPR17 with a small-molecule agonist. Sci. Signal. *6*, ra93.

Herce, H.D., Rajan, M., Lättig-Tünnemann, G., Fillies, M., and Cardoso, M.C. (2014). A novel cell permeable DNA replication and repair marker. Nucleus (Austin, Tex.) *5*, 590–600.

Jänicke, R.U., Sprengart, M.L., Wati, M.R., and Porter, A.G. (1998). Caspase-3 is required for DNA fragmentation and morphological changes associated with apoptosis. J. Biol. Chem. *273*, 9357–9360.

Jung, S.-H., Kim, S., Chung, A.-Y., Kim, H.-T., So, J.-H., Ryu, J., Park, H.-C., and Kim, C.-H. (2010). Visualization of Myelination in GFP-Transgenic Zebrafish. Dev. Dynam.: an official publication of the American Association of Anatomists *239*, 592–597.

Karttunen, M.J., Czopka, T., Goedhart, M., Early, J.J., and Lyons, D.A. (2017). Regeneration of myelin sheaths of normal length and thickness in the zebrafish CNS correlates with growth of axons in caliber. PLoS One *12*, e0178058.

Kirby, B.B., Takada, N., Latimer, A.J., Shin, J., Carney, T.J., Kelsh, R.N., and Appel, B. (2006). *In vivo* time-lapse imaging shows dynamic oligodendrocyte progenitor behavior during zebrafish development. Nat. Neurosci. *9*, 1506–1511.

Koudelka, S., Voas, M.G., Almeida, R.G., Baraban, M., Soetaert, J., Meyer, M.P., Talbot, W.S., and Lyons, D.A. (2016). Individual neuronal subtypes Exhibit Diversity in CNS myelination mediated by synaptic vesicle release. Curr. Biol. *26*, 1447–1455.

Kucenas, S., Snell, H., and Appel, B. (2008). nkx2.2a promotes specification and differentiation of a myelinating subset of oligodendrocyte lineage cells in zebrafish. Neuron Glia Biol. *4*, 71–81.

Laselva, O., Erwood, S., Du, K., Ivakine, Z., and Bear, C.E. (2019). Activity of lumacaftor is not conserved in zebrafish Cftr bearing the major cystic fibrosis-causing mutation. FASEB Bioadv. *1*, 661–670.

Lassmann, H., and Bradl, M. (2017). Multiple sclerosis: experimental models and reality. Acta Neuropathol. *133*, 223–244.

Lubetzki, C., Zalc, B., Williams, A., Stadelmann, C., and Stankoff, B. (2020). Remyelination in multiple sclerosis: from basic science to clinical translation. Lancet Neurol. *19*, 678–688.

Marinelli, C., Bertalot, T., Zusso, M., Skaper, S.D., and Giusti, P. (2016). Systematic review of pharmacological properties of the oligodendrocyte lineage. Front. Cell. Neurosci. *10*, 27.

Merten, N., Fischer, J., Simon, K., Zhang, L., Schröder, R., Peters, L., Letombe, A.-G., Hennen, S., Schrage, R., Bödefeld, T., et al. (2018). Repurposing HAMI3379 to block GPR17 and promote rodent and human oligodendrocyte differentiation. Cell Chem. Biol. *25*, 775–786.e5.

Moffat, J.G., Vincent, F., Lee, J.A., Eder, J., and Prunotto, M. (2017). Opportunities and challenges in phenotypic drug discovery: an industry perspective. Nat. Rev. Drug Discov. *16*, 531–543.

Mogha, A., D'Rozario, M., and Monk, K.R. (2016). G protein-coupled receptors in myelinating glia. Trends Pharmacol. Sci. *37*, 977–987.

Müller, C.E., Pegurier, C., Deligny, M.L.R., El-Tayeb, A., Hockemeyer, J., Ledecq, M., Mercier, J., Provins, L., Boshta, N.M., Bhattarai, S., et al. (2018). (aza)indole-, benzothiophene-, and benzofuran-3-sulfonamides. Patent WO-2018122232-A1 (Word Intellectual Property Organization).

Münzel, E.J., Schaefer, K., Obirei, B., Kremmer, E., Burton, E.A., Kuscha, V., Becker, C.G., Brösamle, C., Williams, A., and Becker, T. (2012). Claudin k is specifically expressed in cells that form myelin during development of the nervous system and regeneration of the optic nerve in adult zebrafish. Glia *60*, 253–270.

Nagarajan, B., Harder, A., Japp, A., Häberlein, F., Mingardo, E., Kleinert, H., Yilmaz, Ö., Zoons, A., Rau, B., Christ, A., et al. (2020). CNS myelin protein 36K regulates oligodendrocyte differentiation through Notch. Glia *68*, 509–527.

Ou, Z., Sun, Y., Lin, L., You, N., Liu, X., Li, H., Ma, Y., Cao, L., Han, Y., Liu, M., et al. (2016). Olig2-Targeted G-protein-coupled receptor Gpr17 regulates oligodendrocyte survival in response to lysolecithin-induced demyelination. J. Neurosci. *36*, 10560–10573.

Patton, E.E., Zon, L.I., and Langenau, D.M. (2021). Zebrafish disease models in drug discovery: from preclinical modelling to clinical trials. Nat. Rev. Drug Discov. *20*, 611–628.

Preston, M.A., and Macklin, W.B. (2015). Zebrafish as a model to investigate CNS myelination. Glia *63*, 177–193.

Satoh, J.-I., Kino, Y., Yanaizu, M., Tosaki, Y., Sakai, K., Ishida, T., and Saito, Y. (2017). Expression of GPR17, a regulator of oligodendrocyte differentiation and maturation. Nasu-Hakola Dis. Brains *6*, 50–54. Intractable & rare diseases research.

Schröder, R., Janssen, N., Schmidt, J., Kebig, A., Merten, N., Hennen, S., Müller, A., Blättermann, S., Mohr-Andrä, M., Zahn, S., et al. (2010). Deconvolution of complex G protein-coupled receptor signaling in live cells using dynamic mass redistribution measurements. Nat. Biotechnol. *28*, 943–949.

Schröder, R., Schmidt, J., Blättermann, S., Peters, L., Janssen, N., Grundmann, M., Seemann, W., Kaufel, D., Merten, N., Drewke, C., et al. (2011). Applying label-free dynamic mass redistribution technology to frame signaling of G protein-coupled receptors noninvasively in living cells. Nat. Protoc. *6*, 1748–1760.

Shin, J., Park, H.-C., Topczewska, J.M., Mawdsley, D.J., and Appel, B. (2003). Neural cell fate analysis in zebrafish using olig2 BAC transgenics. Methods Cell Sci. *25*, 7–14.

Shukla, A., Kaur, P., Narayanan, D.L., do Rosario, M.C., Kadavigere, R., and Girisha, K.M. (2021). Genetic disorders with central nervous system white matter abnormalities: an update. Clin. Genet. *99*, 119–132.

Simon, K., Hennen, S., Merten, N., Blättermann, S., Gillard, M., Kostenis, E., and Gomeza, J. (2016). The orphan G protein-coupled receptor GPR17 negatively regulates oligodendrocyte differentiation via Gαi/o and its downstream effector molecules. J. Biol. Chem. *291*, 705–718.

Simon, K., Merten, N., Schröder, R., Hennen, S., Preis, P., Schmitt, N.-K., Peters, L., Schrage, R., Vermeiren, C., Gillard, M., et al. (2017). The orphan receptor GPR17 is unresponsive to Uracil nucleotides and cysteinyl leukotrienes. Mol. Pharmacol. *91*, 518–532.

Takada, N., and Appel, B. (2010). Identification of genes expressed by zebrafish oligodendrocytes using a differential microarray screen.

Dev. Dynam.: an official publication of the American Association of Anatomists *239*, 2041–2047.

Taylor, K.L., Grant, N.J., Temperley, N.D., and Patton, E.E. (2010). Small molecule screening in zebrafish: an *in vivo* approach to identifying new chemical tools and drug leads. Cell Commun. Signal. *8*, 11.

Turan, F., Yilmaz, Ö., Schünemann, L., Lindenberg, T.T., Kalanithy, J.C., Harder, A., Ahmadi, S., Duman, T., MacDonald, R.B., Winter, D., et al. (2021). Effect of modulating glutamate signaling on myelinating oligodendrocytes and their development-A study in the zebrafish model. J. Neurosci. Res. *99*, 2774–2792.

Wan, Q.-F., Zhou, Z.-Y., Thakur, P., Vila, A., Sherry, D.M., Janz, R., and Heidelberger, R. (2010). SV2 acts via presynaptic calcium to regulate neurotransmitter release. Neuron *66*, 884–895.

Wang, J., He, X., Meng, H., Li, Y., Dmitriev, P., Tian, F., Page, J.C., Lu, Q.R., and He, Z. (2020). Robust myelination of regenerated axons induced by combined manipulations of GPR17 and microglia. Neuron *108*, 876–886.e4.

## STAR★METHODS

### KEY RESOURCES TABLE

| REAGENT or RESOURCE | SOURCE | IDENTIFIER |
|---|---|---|
| Antibodies | | |
| Mouse anti-HA | Roche | Cat# 11583816001; RRID: AB_514505 |
| Goat anti-mouse IgG antibody HRP | Sigma-Aldrich | Cat# A4416; RRID: AB_258167 |
| Goat anti-mouse-Cy2, Millipore AP124J | Millipore | Cat# AP124J; RRID: AB_92461 |
| Mouse anti-rat MBP | LifeSpan BioSciences | Cat# LS-B8056 |
| Rabbit anti-β-actin | BioLegend | Cat# 622102; RRID: AB_315946 |
| Goat anti-rabbit IgG antibody HRP | Antibodies-Online | Cat# ABIN102010; RRID: AB_10762386 |
| Mouse anti-Pcna | Sigma-Aldrich | Cat# P8825; RRID: AB_477413 |
| Rabbit anti-Cleaved caspase 3 | Cell signaling Technologies | Cat# 9661; RRID: AB_2341188 |
| Mouse anti-Sv2 | DSHB | Cat#SV2; RRID: AB_2315387 |
| Mouse anti-acetylated tubulin | Sigma-Aldrich | Cat# T7451; RRID: AB_609894 |
| Goat anti-mouse Alexa Fluor 546 | Life Technologies | Cat# A-11030; RRID: AB_2534089 |
| Goat anti-mouse-HRP | Jackson Immuno Research | Cat# 115-035-003; RRID: AB_10015289 |
| Goat anti-rabbit Alexa Fluor 488 | Life Technologie | Cat# A-11034; RRID: AB_2576217 |
| Goat anti-rabbit-HRP | Jackson Immuni Research | Cat# 111-035-144; RRID: AB_2307391 |
| Chemicals, peptides, and recombinant proteins | | |
| MDL29,951 | Maybridge | Cat# SEW06645 |
| DMEM | Thermo Fisher Scientific | Cat# 41965062 |
| DMEM/F12 | Thermo Fisher Scientific | Cat# 31330095 |
| FBS | PAN biotech | Cat# P30-3702 |
| G418 | InvivoGen | Cat# ant-gn-5 |
| Hygromycin B | InvivoGen | Cat# ant-hg-5 |
| Blasticidin | InvivoGen | Cat# ant-bl-1 |
| Doxycycline | Sigma-Aldrich | Cat# D9891 |
| Neurobasal medium | Thermo Fisher Scientific | Cat# 21103049 |
| B27 | Thermo Fisher Scientific | Cat# 17504044 |
| GlutaMAX | Thermo Fisher Scientific | Cat# 35050038 |
| PDGF-AA | PeproTech | Cat# 100-13A-50UG |
| bFGF | PeproTech | Cat# 100-18B-50UG |
| CNTF | PeproTech | Cat# 450-50-25UG |
| Triiodothyronine (T3) | Sigma-Aldrich | Cat# T2752 |
| poly-L-ornithine | Sigma-Aldrich | Cat# P3655 |
| poly-D-lysine | Sigma-Aldrich | Cat# P2636 |
| Hanks' buffered salt solution (HBSS) | Thermo Fisher Scientific | Cat# 14175129 |
| Isobutylmethylxanthine (IBMX) | Sigma-Aldrich | Cat# I5879 |
| Forskolin | Bachem | Cat# TRC-F701800 |
| Fugene HD | Promega | Cat# E2311 |
| TMB | Promega | Cat# W4121 |
| TRIzol Reagent | Ambion by Life Technologies | Cat# T9424 |
| Mowiol solution | Sigma-Aldrich | Cat# 81381 |
| MS222 | Fluka Analytical | Cat# A5040 |
| DreamTag® DNA Polymerase | Thermo Fisher Scientific | Cat# EP0701 |
| Critical commercial assays | | |
| FLIPR® Calcium 5 Assay kit | Molecular Devices | Cat# R8186 |
| HTRF-cAMP dynamic 2 kit | Cisbio International | Cat# 62AM4PEC |
| Pierce BCA Protein Assay | Thermo Fisher Scientific | Cat# 23225 |

(*Continued on next page*)

*Continued*

| REAGENT or RESOURCE | SOURCE | IDENTIFIER |
|---|---|---|
| ECL Prime Western blotting detection reagent | GE Healthcare | Cat# RPN2236 |
| 5′/3′ RACE Kit, 2nd Generation | Roche Life Science | Cat# 3353621001 |
| NucleoSpin Gel and PCR Clean-UP | Macherey-Nagel | Cat#740609.250 |
| iScript Reverse Transcription Supermix | Biorad | Cat# 1708841 |
| RNAscope Fluorescent Multiplex Reagent Kit | Acdbio | Cat# 320850 |
| pGEM®-T Easy Vector Systems I | Promega | Cat# A1360 |
| TRIzol RNA Isolation | Invitrogen | Cat# 15596018 |
| mMessage mMachine T7 Ultra Kit | Invitrogen | Cat# AM1345 |
| Qubit RNA HS Assay Kit | Life Technologies | Cat# Q32852 |
| **Experimental models: Cell lines** | | |
| HEK293 | ATCC | Cat# CRL-1573 |
| h-CYSLTR1-HEK293 | Simon et al., 2017 | N/A |
| h-P2RY1-1321N1 | Hennen et al., 2013 | N/A |
| h-P2RY12-1321N1 | Simon et al., 2017 | N/A |
| h-P2RY13-1321N1 | Hennen et al., 2013 | N/A |
| h-P2RY14-HEK293 | Simon et al., 2017 | N/A |
| h-GPR17-CHO | Hennen et al., 2013 | N/A |
| **Experimental models: Organisms/strains** | | |
| Wistar rat | Charles river | Strain code: 003 |
| TU wildtype fishline | EZRC, KIT | Cat# 1173 |
| TL wildtype fishline | EZRC, KIT | Cat# 1174 |
| AB wildtype fishline | EZRC, KIT | Cat# 1175 |
| *Tg(olig2:EGFP)* | Shin et al., 2003 | N/A |
| *Tg(claudinK:EGFP)* | Münzel et al., 2012 | N/A |
| *Tg(mbp:EGFP)* | Almeida et al., 2011 | N/A |
| *Tg(nkk2.2a:mEGFP)* | Kirby et al., 2006; Kucenas et al., 2008 | N/A |
| **Oligonucleotides** | | |
| GSP1: 5′-GTTGAGCCATTGACTTCTAC-3′ | This paper | N/A |
| GSP2: 5′-GCCATAGACACAATCACCAA-3′ | This paper | N/A |
| GSP3: 5′-ACCACAGCAAGGTATCTGTC-3′ | This paper | N/A |
| RT-PCR *gpr17* forward primer (exon 1): 5′-CTAGGAAACTGCACAACTC-3′ | This paper | N/A |
| RT-PCR *gpr17* reverse primer (exon 2): 5′-GGAAGTTCTGTCAAGGAG-3′ | This paper | N/A |
| RT-PCR *eef1a1l1* forward primer: 5′-GGAGTGATCTCTCAATCTTG-3′ | Nagarajan et al., 2020 | N/A |
| RT-PCR *eef1a1l1* reverse primer: 5′-CTTCCTTCTCGAACTTCTC-3′ | Nagarajan et al., 2020 | N/A |
| *gpr17* forward: 5′-CTTGCTGCCCAACCAGTCCA-3′ | This paper | N/A |
| *gpr17* reverse: 5′-AGCGAGGAGGTAAGACGGTT-3′ | This paper | N/A |
| *gpr17*-geno-forward primer 5′-AACTGGAGGTCATTGGCC-3′ | This paper | N/A |
| *gpr17*-geno-reverse primer 5′-CATACGGTTGAGCCATTGAC-3′ | This paper | N/A |
| **Recombinant DNA** | | |
| h-GPR17-pcDNA3.1 (+) | Hennen et al., 2013 | N/A |

(*Continued on next page*)

*Continued*

| REAGENT or RESOURCE | SOURCE | IDENTIFIER |
|---|---|---|
| zf-Gpr17-pcDNA3.1 (+) | This paper | N/A |
| h/zf-GPR17-pcDNA3.1 (+) | This paper | N/A |
| zf/h-Gpr17-pcDNA3.1 (+) | This paper | N/A |
| **Software and algorithms** | | |
| ZEN software | Zeiss | https://www.zeiss.de/mikroskopie/downloads/zen.html |
| Gelscan software | Bioscitec | https://www.biosctec.de |
| Fiji is just ImageJ (Fiji) | National Institutes of Health | http://imagej.nih.gov/ij/ |
| Fiji ImageJ Cell Counter | Kurt de Vos (University of Sheffield) | https://imagej.nih.gov/ij/plugins/cell-counter.html |
| GraphPad | Prism | https://www.graphpad.com/scientific-software/prism/ |
| BioRender | BioRender | https://biorender.com/ |
| **Other** | | |
| Black 384-well plates with clear bottoms | Greiner | Cat# 781091 |
| Black 384-well plates | Greiner | Cat# 781076 |
| 384-well fibronectin-coated EPIC biosensor plates | Corning | Cat# 5042 |

## RESOURCE AVAILABILITY

### Lead contact

Further information and requests for resources and reagents should be directed to and will be fulfilled by the Lead Contact, Evi Kostenis (kostenis@uni-bonn.de).

### Materials availability

All unique/stable reagents generated in this study are available from the Lead Contact with a completed Materials Transfer Agreement.

### Data and code availability

- All data reported in this paper will be shared by the lead contact upon request.
- This paper does not report original code.
- Any additional information required to reanalyze the data reported in this paper is available from the lead contact upon request.

## EXPERIMENTAL MODEL AND SUBJECT DETAILS

### Zebrafish housing and maintenance

Adult zebrafish (males and females) were maintained at 28°C with a light/dark cycle of 14/10 h under actual husbandry license (§ 11, City of Bonn, Germany). Embryos were gained by natural spawning and kept until ≤5 days post fertilization (dpf) at 28°C in an incubator in 0.3× Danieau's buffer (1× Danieau's buffer: 58 mM NaCl, 0.7 mM KCl, 0.4 mM $MgSO_4$, 0.6 mM $Ca(NO_3)_2$, 5 mM HEPES, pH 7.2). Until 24 hpf, 0.3× Danieau's buffer was supplemented with 0.00001% methylene blue solution. From 24 hpf, when used for imaging, 0.3 × Danieau's buffer was supplemented with 0.003% phenylthiourea (PTU) to prevent pigmentation (Danieau/PTU solution). All experiments were done according to institutional and national law, following ARRIVE guidelines (https://www.nc3rs.org.uk/arrive-guidelines).

### Cell lines

Human embryonic kidney cells (HEK 293), originating from a female fetus, were obtained from the American Type Culture Collection (ATCC) and cultured in Dulbecco's Modified Eagle Medium (DMEM, ThermoFisher) containing 10% fetal bovine serum (FBS, PAN biotech), 100 U $ml^{-1}$ Penicillin, 100 mg $mL^{-1}$ Streptomycin (ThermoFisher) at 37°C and 5% $CO_2$. For h-P2RY14-HEK293, h-CYSLTR1-HEK293, h-P2RY1-1321N1, h-P2RY12-1321N1, and h-P2RY13-1321N1 the medium was supplemented with G418 (500 μg/mL for HEK293 and 800 μg/mL for 1321N1) (InvivoGen). Flp-In T-REx CHO cells stably expressing h-GPR17 (h-GPR17-CHO) were cultivated in DMEM with Nutrient Mixture F-12 (DMEM/F12) supplemented with 10% FBS, penicillin (100 U $ml^{-1}$), streptomycin (100 μg $mL^{-1}$), complemented with hygromycin B (500 μg $mL^{-1}$) and blasticidin (30 μg $mL^{-1}$) (both InvivoGen). Expression of

h-GPR17 was induced by treatment with doxycycline (1 μg $mL^{-1}$) for 14 to 20 h. For transient transfection of receptor cDNAs, Fugene HD (Promega) was used according to manufacturer's instructions.

Primary rat OPCs were isolated by a differential detachment method from mixed glial cultures prepared from neonatal Wistar rat cerebra (mixed male and female brains), as previously described (Simon et al., 2016). OPCs were seeded in proliferation medium (Neurobasal medium supplemented with 2% (v/v) B27, 2 mM GlutaMAX, 100 units/ml penicillin, 100 mg/mL streptomycin, 10 ng/mL platelet-derived growth factor-AA (PDGF-AA, PeproTech) and 10 ng/mL basic fibroblast growth factor (bFGF, PeproTech). For induction of spontaneous *in vitro* differentiation and GPR17 protein expression, medium was switched to growth factor-free Neurobasal medium. For terminal differentiation and quantification of myelin basic protein (MBP) expression, after 24 h the growth factor-free medium was supplemented with 0.20 ng/mL triiodothyronine (T3) and 10 ng/mL ciliary neurotrophic factor (CNTF, PeproTech) together with the analyzed compounds for additional 2–3 days.

## METHOD DETAILS

### DNA constructs

For DNA sequencing, the coding sequence of zebrafish *zf-gpr17* was amplified by PCR from genomic DNA and inserted into the cloning vector pBluescript II SK(−) (Agilent) via 5′ HindIII and 3′ XhoI. For analyses in HEK 293 cells, *zf-gpr17* and the chimeric receptors *h/zf-GPR17* and *zf/h-gpr17* were *de novo* synthesized and cloned into pcDNA 3.1 (+) by GeneCust. For ELISA and immunofluorescence experiments, a triple HA tag (3xHA; 3xYPYDVPDYA) was introduced at the N terminus.

### Enzyme-linked Immunosorbent assay (ELISA)

24 h after transfection, cells were seeded in poly-D-lysine-coated 96-well plates at a density of 50,000 cells/well. Next day, cells were fixed with 4% paraformaldehyde (PFA) for 20 min, washed three times with phosphate-buffered saline (PBS), and blocked with blocking buffer (3% dry milk, 50 mM Tris-HCl, pH 7.5). Cells were incubated with the monoclonal mouse anti-HA antibody (Roche 11583816001) diluted 1:400 in blocking buffer for 1 h at 37°C. Cells were washed three times with PBS for 15 min at 37°C and then the secondary antibody (anti- mouse HRP-conjugated, Sigma-Aldrich A4416) diluted 1:1,000 in blocking buffer was incubated for 1 h in the dark at 37°C. After washing three times with PBS for 5 min at 37°C, 100 μL 3,3′,5,5′-Tetramethylbenzidin (TMB, Promega) solution was added to each well and incubated for 3–5 min. Reaction was stopped by adding 50 μL of 0.5 M $H_2SO_4$ to each well. Absorbance was measured at 450 nm with 620 nm reference wavelength at the TECAN sunrise absorbance reader (TECAN).

### Immunocytochemistry

Cells were transfected, seeded on poly-D-lysine-treated coverslips in 24-well plates and grown overnight at 37°C and 5% $CO_2$. Cells were fixed in 4% PFA in PBS for 30 min at room temperature (RT). After three washing steps with 500 μL PBS for 15 min at 37°C, cells were incubated with 300 μL of ICC blocking buffer 10 % normal goat serum (NGS)/1 % Bovine serum albumin (BSA)/PBS for 1 h at 37°C. Blocking buffer was replaced with the primary antibody (mouse anti-HA) diluted 1:500 in ICC blocking solution. After an incubation of 1 h at 37°C, and three washing steps with PBS, the secondary antibody (goat anti-mouse-Cy2, Millipore AP124J) diluted 1:500 in blocking buffer was added to the wells. Cells were incubated for 1 h at 37°C, subsequently washed three times with PBS, and counterstained with DAPI solution (0.2 μg $mL^{-1}$) for 15 min in the dark at RT. Following three washes with PBS cells were mounted in Mowiol solution (Sigma-Aldrich). Labelled cells were analyzed with an Apotome Observer Z.1 inverted fluorescence microscope (Zeiss) with ZEN software, Receptors were visualized using the GFP/Cy2 filter set and nuclei with the DAPI filter set.

### $Ca^{++}$mobilization assay

Intracellular calcium mobilization was quantified with the Calcium 5 Assay kit and the FlexStation 3 Multimode Microplate Reader or the FLIPR Tetra System according to the manufacturer's instructions. Briefly, h-GPR17-CHO cells were defrosted and seeded at a density of 20,000 cells/well into a black 384 well plate with clear bottom. 16–20 h after seeding cells were loaded with Calcium 5 dye for 60 min. Fluorescent signal was recorded over time ("baseline read") before cells were preincubated for 30 min with increasing concentration of 6-chloro-N-[5-(cyanomethyl)-3-fluoro-6-methoxypyridin-2-yl]-1H-indole-3-sulfonamide (UCB6651; compound I-255 in (Müller et al., 2018), 6-chloro-N-(2-methylpyridin-4-yl)-1H-indole-3-sulfonamide (EMI280422) or vehicle (DMSO) in assay buffer (Hanks' buffered salt solution (HBSS) supplemented with 20 mM HEPES, pH 7.4). After this incubation time, 50 nM GPR17 agonist MDL29,951 ($EC_{80}$) was added to the cells and fluorescent signal was measured to determine the inhibitory effect of the test compounds.

### HTRF-based cAMP Accumulation assay

The assays were performed in black 384-well plates with 5,000 h-GPR17-CHO cells per well. Cells were preincubated for 30 min with varying concentrations of UCB6651 or vehicle (DMSO) before a fixed concentration of 10 nM MDL29,951 ($EC_{90}$) was added in a final volume of 20 μL HBSS supplemented with 20 mM HEPES (pH 7.4) containing 5 μM forskolin and 0.1 mM IBMX. After 60 min incubation at room temperature the reaction was terminated by lysis using the cAMP dynamic2 kit from Cisbio according to the manufacturer's instructions. The level of cAMP was then determined by measuring the fluorescence ratio (665 nm/620 nm) using an Envision plate reader with laser excitation.

### Label-free dynamic mass redistribution (DMR) assays

DMR was recorded as described previously in detail (Schröder et al., 2010, 2011). Briefly, cells were seeded (HEK293 18,000 cells/well, CHO and 1321N1 15,000 cells/well) in 384-well fibronectin-coated EPIC biosensor plates (Corning) and grown overnight. On the assay day, cells were washed twice with HBSS containing 20 mM HEPES adjusted to final DMSO content and incubated for 1 h at 28°C in the EPIC benchtop reader (Corning). The sensor plate was scanned for a baseline read for about 5 min and then buffer or UCB6651 was added with a semi-automated liquid handling system (Selma, CyBio). After a 30 min antagonist read, MDL29,951 was added with a semi-automated liquid handling system (Selma, CyBio) and DMR changes were recorded for 1 h. To estimate potency of UCB6651 on h-GPR17-CHO, 1 μM MDL29,951 (first $EC_{80}$ of biphasic agonist curve) was used. Quantification of buffer corrected DMR signals was performed by calculation of the maximum response or the area under the curve (AUC) between 0 and 3,600 s or 0 and 900 s.

### Western blotting

OPCs were seeded in proliferation medium into poly-L-ornithine-coated 12-well tissue culture plates (80,000–100,000 cells per well). After induction of GPR17 expression and terminal differentiation of oligodendrocytes in the presence of UCB6651 for 2–3 days, cells were washed twice with ice-cold PBS and lysed in ice-cold lysis buffer (25 mM Tris, pH 7.4, 150 mM NaCl, 1 mM EDTA, 1% Triton X-100, 1% IGEPAL) supplemented with protease inhibitor mixture (Sigma-Aldrich). Lysates were rotated for 20 min at 4°C and centrifuged at 13,200 rpm at 4°C for 10 min. Protein concentration was determined using the Pierce BCA Protein Assay (Thermo Fisher Scientific) according to manufacturer's instructions. 7.5–15 μg of protein were separated by 10% NuPAGE bis-tris gel electrophoresis (Thermo Fisher Scientific) and transferred to nitrocellulose membrane (HybondTM-C Extra, GE Healthcare) by wet blotting (XCell II Blot Module, Thermo Fisher Scientific). After washing, membranes were blocked with Roti-Block (1x; Carl Roth) for 1 h at room temperature and incubated overnight at 4°C in Roti-Block with mouse anti-MBP antibody (1:5,000; LifeSpan BioSciences) and rabbit anti-β-actin (1:2,500; BioLegend) to normalize for equal loading and protein transfer. Membranes were washed 3 times with PBS containing 0.1% Tween and then incubated for 1 h at room temperature with corresponding horseradish peroxidase-conjugated secondary antibody (goat anti-rabbit IgG antibody HRP (1:10,000; antikoerper-online), goat anti-mouse IgG antibody HRP (1:10,000; Sigma-Aldrich)) in Roti-Block. The immunoreactive proteins were visualized by chemiluminescence using Amersham Biosciences ECL Prime Western blotting detection reagent (GE Healthcare) and quantified by densitometry using Gelscan software (Bioscitec).

### Rapid amplification of 5′cDNA ends (5′ RACE)

Total RNA was prepared from a pool of 50 wt zebrafish larvae using TRIzol RNA Isolation. The 5′ RACE procedure strictly followed the instruction manual (5′/3′ RACE Kit, second Generation; Roche). First-strand cDNA was synthesized from 1 μg of total RNA using the *gpr17* gene-specific primer 1 (GSP1: 5′-GTTGAGCCATTGACTTCTAC). Race-ready cDNA was amplified by polymerase chain reaction (PCR) using the GSP2 (5′-GCCATAGACACAATCACCAA). Second PCR reaction was performed using the GSP3 (5′-ACCACAGCAAGGTATCTGTC). PCR products from the second PCR reaction were run on 1% agarose gel and the band obtained was purified using the NucleoSpin Gel and PCR Clean-up kit (Macherey-Nagel) and sequenced.

### Exon-exon junction reverse transcription polymerase chain reaction (RT-PCR)

Total RNA was extracted from 30 wt larvae at different dpf using TRIzol RNA Isolation. 1 μg total RNA was reverse transcribed using iScript Reverse Transcription Supermix for RT-PCR (Biorad 1708841) and after 5 min denaturation at 95°C, 30 amplification cycles were carried out: 30 s at 95°C and 30 s at 60°C. *gpr17* forward primer (exon 1): 5′-CTAGGAAACTGCACAACTC; *gpr17* reverse primer (exon 2): 5′-GGAAGTTCTGTCAAGGAG. *eef1a1l1* forward primer: 5′-GGAGTGATCTCTCAATCTTG; *eef1a1l1* reverse primer: 5′-CTTCCTTCTCGAACTTCTC.

### Tissue preparation and *in situ* hybridization

Zebrafish larvae were anesthetized with 600 μM ethyl 3-aminobenzoate methanesulfonate (MS222; Sigma Aldrich A5040) in Danieau/PTU solution and immersion fixed for 2 h at RT in 4% paraformaldehyde (PFA). Zebrafish younger than 3 dpf were previously dechorionated using 2 mg/mL pronase in Danieau/PTU solution for 10 min at RT. Larvae were washed with PBS 3 × 15 min, dehydrated through a series of methanol, and stored in methanol at RT for 2 h. For *in situ* hybridization, we used the RNAscope® Fluorescent Multiplex Reagent Kit (ACD 320850) according to the manufacturer's protocol for fixed samples. RNA probe against zebrafish *gpr17* was purchased from ACD (ACD, 300031). Larvae were finally mounted in agarose and imaged with a two-photon microscope (LaVision BioTec, TriMScope™ II). Image processing was performed using Fiji ImageJ.

### Generation of *gpr17* mutant line

Design of sgRNA targeting *gpr17*, founder identification and delivery of F1 animals was performed by Nanjing Sanjay Medical Technology Co (China) after payment of the corresponding technical service fees. To identify mutated alleles in F1 animals, DNA from adult fin clips was extracted and amplified by PCR using the *gpr17* forward (5′-CTTGCTGCCCAACCAGTCCA-3′) and *gpr17* reverse (5′-AGCGAGGAGGTAAGACGGTT-3′) primers. PCR was done with Dream Tag Polymerase (Thermo Fisher Scientific EP0701) and conditions were as follows: 95°C for 3 min, followed by 25 cycles at 95°C for 30 s, 71°C for 30 s and 72°C for 1 min. Final extension was at 72°C for 10 min. The PCR products were cleaned up using the NucleoSpin Gel and PCR Clean-UP Kit (Macherey Nagel) and

subsequently TA cloned into pGEM-T Easy vector (Promega). Clones were sequenced and aligned to wt genomic DNA using BLAST global alignment tool.

### Genotyping of the *gpr17* knockout line Δ43

Genomic DNA was extracted and amplified by PCR using the *gpr17*-geno-forward primer 5′-AACTGGAGGTCATTGGCC-3′ and the *gpr17*-geno-reverse primer 5′-CATACGGTTGAGCCATTGAC-3′. After 3 min denaturation at 95°C, 25 amplification cycles were carried out: 30 s at 95°C, 30 s at 63°C and 1 min at 72°C. Final extension was at 72°C for 10 min. The amplified products were separated on a 2 % agarose gel. The wild-type allele resulted in a 267-bp band, whereas homozygous Δ43 allele with a deletion of 43 bp resolved in a 224-bp product. Heterozygous DNA resolved in two bands at 267 and 224 bp.

### Morpholino injections

Antisense morpholino (MO) oligonucleotides (Gene Tools) were dissolved in distilled water to 2 mM stock concentrations. A working concentration of 0.25 mM was used for *gpr17* MO (GTTCTGTCAAGGAGGACTCCATTT) and control MO (CCTCTTACCT CAGTTACAATTTATA). A glass micropipette was filled with the MO working solution (distilled water, 4 mg/mL phenol red, diluted MO) and a volume of 1.3 nL was injected into the yolk of one-cell stage embryos.

### mRNA injections

For *in vitro* synthesis of *zf-gpr17*, *h-GPR17*, *h/zf-GPR17* and control *tdTomato* mRNAs, mMESSAGE mMACHINE T7 Ultra Kit (Thermo Fisher Scientific) was used according to the manufacturer's instructions. mRNAs were precipitated with lithium chloride, quantified with the Qubit RNA HA Assay Kit (Life Technologies) and frozen as aliquots at −80°C. Injections of mRNA into *gpr17-Δ43* embryos were performed at the one cell stage. A 1.8 nL volume containing 200 pg of mRNA in Ampuwa water was used.

### Immunohistochemistry

For paraffin section studies, larvae were anesthetized by immersing in MS222 solution, followed by immersion in 4% PFA in PBS for 2 h and embedded in paraffin. Sections were counterstained with hematoxylin. Staining with respective antibodies using Ventana Benchmark XT Automated IHC/slide staining system (Roche) was performed at the following dilutions: anti-Pcna (Sigma), 1:1,000; anti-Cleaved caspase 3 (Cell signaling Technologies), 1:200. Images were acquired with the Nikon AZ100 microscope and processed with Fiji ImageJ.

For larval whole mount staining, larvae were anesthetized by immersing in MS222 solution, followed by immersion in 4% PFA in PBS for 2 h at RT. Afterwards, larvae were washed with PBS 3 × 15 min, dehydrated through a series of methanol and followed by rehydration. Embryos were then washed 3 times for 5 min in PBS- 0.1% Tween 20 (PBST), equilibrated in Tris buffer (150 mM Tris-HCl pH 9.0) at 70°C for 15 min, permeabilized with 5 μg/mL ProteinaseK in PBST for 90 min at RT, fixed again in 4% PFA for 20 min, and blocked in 10% normal goat serum (NGS)/2% Bovine serum albumin (BSA)/PBST at 4°C for 4 h. Larvae were then incubated in primary antibody solution 2% NGS/2% BSA/PBST at 4°C for 72 h with the following antibodies: anti-Sv2 (deposited to DSHB by Buckley, K.M. AB_2315387), 1:250; and anti-acetylated tubulin (Sigma-Aldrich), 1:500. First antibody incubation was stopped with 5 washing steps in PBST at RT before incubation with the respective secondary antibody at 4°C for 48 h. The following antibodies were used: anti-mouse Alexa Fluor 546 and anti-rabbit Alexa Fluor 488 (Life Technologies); anti-mouse-HRP and anti-rabbit-HRP (Jackson ImmunoResearch). Incubations were stopped and unbound antibody was removed with 6 washing steps for 15 min and 5 washing steps for 5 min with PBST at RT followed by a post fixation with 4% PFA for 20 min at RT. Fixation solution was removed with five washing steps with 1xPBST for 5 min. Stained larvae were then mounted in agarose for two-photon imaging.

### Imaging

For fluorescent images, a two-photon imaging with a scan head based laser-scanning microscope TriM Scope$^{(Tm)}$ (LaVision, BioTec, Bielefeld, Germany) equipped with a 20x water-immersion objective lens (NA1.0, W Plan-Apochromat, Zeiss) and a tuneable TiSa laser (InSigh Deepse, Spectra-Physics, Santa Clara, USA) was used. Zebrafish embryos and young larvae were anaesthetized in MS222. Zebrafish younger than 3 dpf were previously dechorionated using 2 mg/mL pronase in 0.3x Danieau for 10 min at RT. Each embryo was arranged to lay laterally and mounted with 200 μL of 1.25% low melting point agarose in 0.3× Danieau. Brightfield images were used to orientate the embryos laterally, anterior to the left, dorsal up. For consistency, bright field and fluorescent images were finally taken from comparable regions of the spinal cord, spanning segments between 4 and 10. Fluorescent images were acquired as z-stacks (z-step, 2 μm) with a field of view of 449 × 111 μm and a resolution of 2730 x 678 pixels, which results in image resolution of 0.16 μm per pixel. Those images taken for cell counting analyses were evaluated using the Fiji (ImageJ) Cell counter plugin (Kurt De Vos, University of Sheffield). Those images taken for fluorescence intensity measurements were acquired with identical conditions (2% laser power) and mean fluorescence intensity from the stitched maximum intensity z-projections was obtained for each fish by using the measurement function of Fiji as previously described (Nagarajan et al., 2020).

### Compound treatment

Zebrafish embryos at 24 hpf were enzymatically dechorionated with 2 mg/mL pronase in Danieau/PTU solution. Embryos were then transferred into small petri dishes filled with or without 0.5 μM UCB6651 or EMI280422 (final concentration) in a total volume of 3 mL of Danieau/PTU solution. The compound solutions were renewed after 24 h.

### Chemical synthesis

Synthesis of 6-chloro-N-[5-(cyanomethyl)-3-fluoro-6-methoxypyridin-2-yl]-1H-indole-3-sulfonamide (UCB6651) was conducted as following (Figure S6): To a solution of 6-chloro-1H-indole-3-sulfonyl chloride (synthesis of the chemical intermediate is reported in Müller et al., 2018; 0.86 g, 3.42 mmol) in pyridine (6 mL) was added 2-(6-amino-5-fluoro-2-methoxy-3-pyridyl)acetonitrile (Müller et al., 2018; 0.25 g, 1.37 mmol) followed by addition of 4-dimethylaminopyridine (0.008 g, 0.07 mmol). The reaction mixture was heated at 100°C for 24 h. After completion, the reaction mixture was evaporated to dryness. The residue was diluted with 2 N HCl (20 mL), water (20 mL) and extracted with ethyl acetate (3 × 25 mL). The organic layer was separated, washed with brine (2 × 30 mL), dried over anhydrous $Na_2SO_4$ and concentrated *in vacuo*. The crude obtained was purified by column chromatography (silica, 100–200 mesh, 35% of ethyl acetate in hexane) to afford 76 mg of 6-chloro-N-[5-(cyanomethyl)-3-fluoro-6-methoxypyridin-2-yl]-1H-indole-3-sulfonamide, as an off-white solid.

Yield: 76 mg (14%); $^1$H NMR (400 MHz, DMSO-$d_6$): δ 12.08 (brs, 1H), 11.02 (brs, 1H), 8.15 (d, $J$ = 2.93 Hz, 1H), 7.85 (d, $J$ = 8.31 Hz, 1H), 7.62 (d, $J$ = 9.78 Hz, 1H), 7.54 (d, $J$ = 1.96 Hz, 1H), 7.22 (dd, $J$ = 8.80, 1.96 Hz, 1H), 3.70 (s, 2H), 3.62 (s, 3H) ; LRMS (ES+) *m/z*: 395 $[M + H]^+$; HRMS (ES+) *m/z*: $[M + H]^+$ calcd 395.0381, found 395.0378.

Synthesis of 6-chloro-N-(2-methylpyridin-4-yl)-1H-indole-3-sulfonamide (EMI280422) was conducted as following (Figure S7): In a sealed vial, 1-(benzenesulfonyl)-6-chloro-indole-3-sulfonyl chloride (Müller et al., 2018; 14 mg, 0.035 mmol) was dissolved in pyridine (0.5 mL) under argon. 4-amino-2-methylpyridine (6 mg, 0.057 mmol) was added and stirred at 85°C overnight. The reaction mixture was evaporated to dryness and purified by basic reverse phase hplc. The residue obtained was readily dissolved in Dioxane (0.75 mL) and water (0.25 mL). Potassium carbonate (15 mg) was added and the reaction mixture was stirred at 100°C for 2 days. The reaction mixture was evaporated to dryness and purified by basic reverse phase hplc.

Yield: 1.7 mg (15%); $^1$H NMR (600 MHz, DMSO-$d_6$): δ 7.94 (m, 2H), 7.83 (d, $J$ = 8.6 Hz, 1H), 7.49 (d, $J$ = 1.9 Hz, 1H), 7.17 (dd, $J$ = 8.6, 1.9 Hz, 1H), 6.88–6.80 (m, 2H), 2.29 (s, 3H); LRMS (ES+) *m/z*: 322 $[M + H]^+$, 320 $[M-H]^-$; HRMS (ES+) *m/z*: $[M + H]^+$ calcd 322.0417, found 322.0422.

## QUANTIFICATION AND STATISTICAL ANALYSIS

All data and statistical analyses were performed with GraphPad Prism software. Data points were fitted to both three-parameter (fixed Hill slope) and four-parameter nonlinear regression isotherms. Concentration–response curves were normalized by setting each experimental maximal effect to 100%. Column statistics were performed with D'Agostino and Pearson omnibus normality test. When comparing two groups, unpaired two-tailed Student's t-tests were used. Comparisons with normalized data (control group set to 100) were analyzed by one-sample, two-sided t-test. One-way ANOVA was performed for multiple groups followed by Tukey's multiple comparisons test. Data are presented as mean ± SD. or SEM. p value significance thresholds were *$p < 0.05$, **$p < 0.01$, ***$p < 0.001$ and ****$p < 0.0001$. See figure legends and text for specific statistical analyses used.